RSC Advances

PAPER

View Article Online
View Journal | View Issue

Cite this: *RSC Adv.*, 2024, **14**, 35239

Design, synthesis, and *in vitro* and *in vivo* biological evaluation of triazolopyrimidine hybrids as multitarget directed anticancer agents†

Heba A. Adawy,[a] Samar S. Tawfik, *[a] Abdullah A. Elgazar,[b] Khalid B. Selim[a] and Fatma E. Goda[a]

Received 17th September 2024
Accepted 29th October 2024

DOI: 10.1039/d4ra06704e

rsc.li/rsc-advances

In response to the urgent need for new anti-proliferative agents, four novel series of triazolopyrimidine compounds (**7a–e**, **9a–d**, **11a–f**, and **13a–e**) were synthesized and evaluated for *in vitro* anticancer efficacy against HCT116, HeLa, and MCF-7 cell lines. Compound **13c** emerged as the most potent, with IC_{50} values of 6.10, 10.33, and 2.42 μM respectively, while **11e** and **7c** also showed strong activity. In multi-target suppression tests, **13c** exhibited the highest inhibition against EGFR, TOP-II, HER-2, and ARO (IC_{50}: 0.087, 31.56, 0.078, and 0.156 μM, respectively). Flow cytometry revealed **13c**'s ability to suppress the S-phase cell population in MCF-7 cells. *In vivo* studies of **13c** demonstrated significant tumor growth inhibition, comparable to the positive control. Molecular docking studies supported the experimental findings, confirming the binding of the novel motifs to the target enzymes' active sites. This comprehensive evaluation highlights the potential of these triazolopyrimidine compounds, particularly **13c**, as promising anticancer agents, warranting further investigation.

1. Introduction

Estrogen-sensitive cancers, particularly breast and cervical cancers, pose significant health challenges globally. Breast cancer is the most common cancer among women worldwide, with over 2.3 million new cases diagnosed in 2020 alone.[1,2] Cervical cancer, while less prevalent in developed countries due to widespread screening and vaccination against human papillomavirus (HPV), remains a major cause of cancer mortality in low- and middle-income countries. These cancers are predicted to continue rising due to aging populations and lifestyle factors. Estrogen-sensitive cancers often show initial responsiveness to hormone therapies; however, the development of resistance remains a critical issue, necessitating more advanced and multifaceted treatment strategies.[3–5]

Epidermal growth factor receptor (EGFR) plays a crucial role in the development and progression of estrogen-sensitive cancers. EGFR is a transmembrane protein that, when activated, triggers signaling pathways promoting cell proliferation, survival, and migration.[6,7] Overexpression or mutation of EGFR is associated with poor prognosis and resistance to conventional therapies. Targeting EGFR with tyrosine kinase inhibitors, such as erlotinib and gefitinib, has shown promise in treating various cancers, including breast cancer.[8] By inhibiting EGFR signaling, these drugs can reduce tumor growth and enhance the effectiveness of other treatments. However, resistance to EGFR inhibitors can still occur, highlighting the need for combination therapies to overcome this challenge.

HER-2 (human epidermal growth factor receptor 2) is another critical target in estrogen-sensitive cancers, particularly in aggressive forms of breast cancer where it is overexpressed. HER-2 promotes cell proliferation and survival through various signaling pathways.[9,10] Targeting HER-2 with monoclonal antibodies like trastuzumab or tyrosine kinase inhibitors such as lapatinib has shown substantial benefits in treating HER-2 positive breast cancers. These therapies can inhibit HER-2 mediated signaling, slowing down or halting tumor growth.[11] However, despite their effectiveness, some patients develop resistance, necessitating the integration of HER-2 targeted therapies with other treatment modalities, including EGFR inhibitors, to improve outcomes.

Aromatase plays a crucial role in estrogen-sensitive cancers by catalyzing the conversion of androgens to estrogens. In postmenopausal women, this enzyme is the primary source of estrogen, and its inhibition can significantly reduce estrogen levels, limiting the growth of estrogen-dependent cancer cells.[12] Aromatase inhibitors, such as anastrozole and letrozole, are commonly used in the treatment of postmenopausal women with hormone receptor-positive breast cancer. Combining aromatase inhibitors with agents targeting EGFR and HER-2 can provide a multifaceted approach to overcoming resistance.[13–15]

[a]*Department of Pharmaceutical Organic Chemistry, Faculty of Pharmacy, Mansoura University, Mansoura 35516, Egypt. E-mail: drsamarelmasry@mans.edu.eg*

[b]*Department of Pharmacognosy, Faculty of Pharmacy, Kafrelsheikh University, Kafr El Sheikh, Egypt*

† Electronic supplementary information (ESI) available. See DOI: https://doi.org/10.1039/d4ra06704e

Topoisomerase II (TOP-II) is an enzyme involved in DNA replication and transcription, playing a pivotal role in cell division. Inhibitors of TOP-II, such as doxorubicin and etoposide, are used to induce DNA damage in cancer cells, leading to apoptosis. These agents could be particularly useful in treating aggressive breast cancers since the expression of TOP-II was linked to poor prognosis.[16–18] Hence, the development of therapeutic agents that could target these enzymes concomitantly could provide a comprehensive strategy to manage estrogen-sensitive cancers and improve patient therapeutic outcomes.

Triazolopyrimidines (TPs) have emerged as a versatile privileged class of compounds with a wide range of biological activities, making them valuable scaffolds in drug design. Notably, TPs have demonstrated significant potential in the treatment of several parasites, neurodegenerative diseases and cardiovascular activities.[19]

Moreover, TPs have been explored for their anticancer properties. For instance, compound **I** exhibited significant activity against CDK2 with an IC_{50} of 0.12 μM after applying scaffold hopping modification on Seliciclib which also lead to improved activity towards GSK-3B and cytotoxicity against HCT-116.[20] Also, compound **II** demonstrated activity against tubulin polymerization with an IC_{50} of 3.8 μM (ref. 21) and potent cytotoxicity against HCT-116 with $IC_{50} = 0.53$ μM. Interestingly, its analogue compound **III** produced pronounced activity against HeLa cells with an IC_{50} of 0.06 μM.[22]

In the same context, compound **IV** displayed potent activity against tyrosyl-DNA phosphodiesterase 2 (TDP2) with an IC_{50} of 22 μM which could be a promising approach in reversing resistance against TOP-II inhibitors.[23] Compound **V** exhibited remarkable potency against lysine specific demethylase 1 (LSD-1), where it achieved an IC_{50} of 1.7 μM and was able to reduce the cell viability of A549 cells in dose dependent manner.[24,25] Compound **VI** showed promising inhibitory activity against CA IX after introducing sulfonamide moiety, with an IC_{50} of 0.0246 μM.

Dawood *et al.* reported the synthesis of compound **VII** which showed moderate cytotoxicity against MCF-7 and was able to inhibit the expression of VEGFR-2 in the cells by 63%.[26] Compound **VIII** showed activity against bromodomain-containing protein 4 (BRD-4) with an IC_{50} of 2.15 μM with strong cytotoxicity against THP-1 with $IC_{50} = 3.86$ μM proving to be promising template for new BRD-4 inhibitors. Compound **IX** was identified using high throughput screening (HTS) as potent inhibitor for cancer cells with highly expressed paired-box gene 2 (PaX-2) and was able to inhibit PaX-2 with an IC_{50} of 1.5 μM.[27]

Compound **X** demonstrated potent activity against methionine aminopeptidase-2 (MetAP-2), with an IC_{50} of 38 nM as a result of implying scaffold hopping to previously reported purine derivatives.[28] Finally, compound **XI** was developed as ERK-3 inhibitor by HTS, where it was found to fit on the ATP pocket allowing it to achieve IC_{50} of 38 nM (Fig. 1).

These findings underscore the potential of triazolopyrimidine-based compounds as modulable scaffolds, capable of targeting diverse enzymes, cellular processes, and cancer cell lines, with IC_{50} values spanning from low nanomolar to micromolar ranges. This could be attributed to their ability to act as bioisostere for adenine similar to afatinib and Qap1, allowing the occupation of ATP active site of several enzymes involved in cancer pathogenesis.[29]

Based on the literature review the development of novel TPs to inhibit multiple targets such as EGFR, Her-2 and TOP-II could be achieved as these enzymes comprise on ATP active sites. In addition, TPs were reported previously as potential aromatase inhibitor[30] like compound **XII** (IC_{50} of 1.1 nm). Moreover, different scaffolds such as oxadiazole (*e.g.* compound **XIII**),[31] 6-aryl-5-cyanothiouracil (*e.g.* compound **XIV**),[32] thiadiazole-urea (*e.g.* compound **XV**),[33] and piperazine (*e.g.* compound **XVI**)[34] were reported as anticancer activity enhancers. All these findings open a way to introduce multi-target anticancer agents through molecular hybridization (Fig. 2).

2. Results and discussion

2.1. Chemistry

The synthesis of the final compounds **7a–e**, **9a–d**, **11a–f** and **13a–e** is illustrated in the following Schemes 1–4. In Scheme 1, the synthesis of 5-methyl-7-(piperazin-1-*yl*)-[1,2,4]triazolo[1,5-*a*] pyrimidine **7a–e**, was accomplished through the following steps. Aminoguanidine bicarbonate (**1**) was reacted with formic acid to yield 3-amino-1,2,4-triazole (**2**). This intermediate (**2**) was then heated with ethyl acetoacetate in acetic acid to produce 5-methyl-[1,2,4]triazolo[1,5-*a*]pyrimidin-7-ol (**3**). The resulting compound was treated with phosphorus oxychloride to obtain the target chloride (**4**) which serves as a key precursor in the following several reactions.[35] The obtained chloride (**4**) was reacted with piperazine in presence of potassium carbonate (K_2CO_3) in dioxane. The resulting product (**5**) was then acylated with chloroacetyl chloride in presence of triethylamine, serving as the base, to yield 4-(2-chloroacetamido)piperazine (**6**). This intermediate was subsequently treated with various piperazine derivatives, morpholine, and piperidine compounds to produce target compounds **7a–e**.

The synthetic strategy for target compounds 1,3,4-thiadiazoles **9a–d**, 1,3,4-oxadiazoles **13a–e**, and pyrimidines **11a–f** involves multiple steps as illustrated in Schemes 2–4. Key intermediates **8a–d** were obtained by reacting 5-amino-1,3,4-thiadiazole-2-thiol with various 4-substituted phenyl isocyanates under reflux, using acetonitrile as solvent (Scheme 2).[36] Additionally, 6-phenyl-2-thiouracil-5-carbonitrile derivatives **10a–f** were synthesized by prolonged heating of different aldehydes with ethyl cyanoacetate and thiourea in ethanol, in presence of K_2CO_3 (Scheme 3). Finally, compounds **8a–d** and **10a–f** were refluxed with (**4**) in acetone/K_2CO_3 to yield our target compounds **9a–d** and **11a–f**, respectively (Schemes 2 and 3).

The synthetic pathway for 1,3,4-oxadiazole-2-thiol intermediates **12a–e** involved the reaction of substituted benzohydrazide with carbon disulfide. The resulting compounds were then heated with (**4**) in dioxane to obtain various oxadiazole derivatives **13a–e**, as illustrated in Scheme 4.

The newly synthesized derivatives (**7a–e**, **9a–d**, **11a–f** and **13a–e**) were characterized using different means of melting point, elemental analysis and spectroscopic data (^{1}H-NMR, ^{13}C-

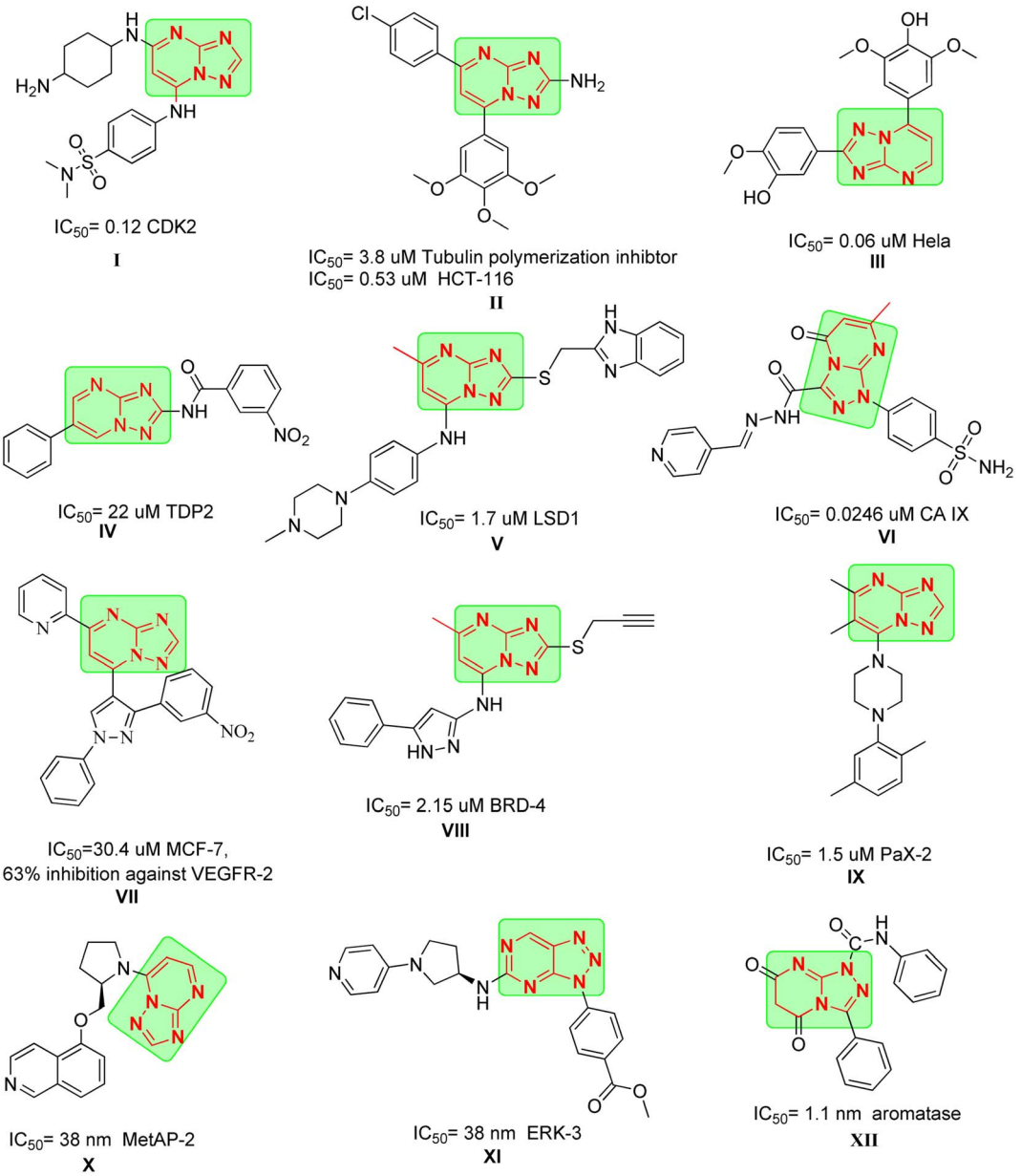

Fig. 1 Examples of anticancer agents containing TPs moiety.

NMR, and MS). ^{1}H-NMR spectra for all the newly synthesized target compounds showed two characteristic singlet signals around 6 and 8 ppm corresponding to two aromatic protons of TP ring. Moreover, compounds **9a–d** and **11a–f** exhibited characteristic singlets corresponding NH protons ranging from 9–11 ppm proving the synthesis of our new targets. In addition, ^{13}C-NMR of compounds **7a–e**, **9a–d** and **11a–f** revealed the appearance of characteristic peak at ~160–169 ppm equivalent to the carbonyl groups. All final targets exhibited a characteristic peak in the aliphatic region at approximately 25 ppm for the methyl substitution of TP moiety. All other data agreed with the suggested structures. The target compounds' mass spectra displayed the correct molecular ion peaks (M^{+}). The experimental section presents the yields and the synthesis procedures.

2.2. Biological activity

2.2.1. *In vitro* analyzing the cytotoxicity activity using HCT-116, HeLa and MCF-7 cell lines. All synthesized compounds were evaluated for their anticancer activity *via* standard MTT assay using three human cancer cell lines: HCT116 (colorectal carcinoma), HeLa (cervical epithelioid carcinoma), and MCF-7 (breast cancer). Doxorubicin was used as a reference drug control. The obtained results revealed variable inhibitory activity across the tested human tumor cell lines. Concerning HCT-116 cell line: compounds **7c**, **11e**, and **13c** demonstrated very strong antitumor activities with IC_{50} values of 7.03, 8.89,

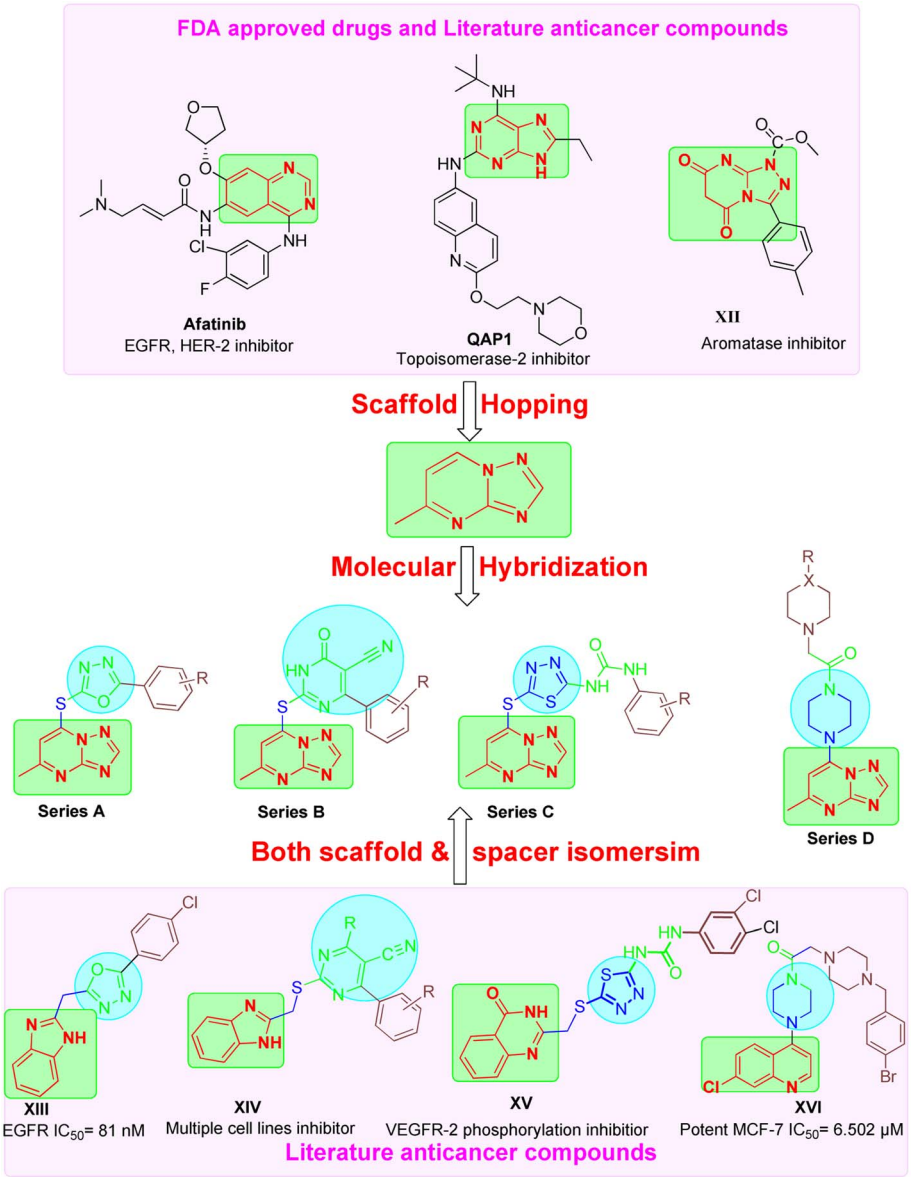

Fig. 2 Design strategy of TPs derivatives as multi target anticancer agents.

and 6.10 μM, respectively. Compounds **11b** and **13a** displayed strong activity with IC_{50} values of 12.61 and 15.03 μM, respectively. Compounds **11c** and **13d** displayed moderate activity with IC_{50} values of 21.51 and 24.79 μM, respectively. HeLa Cell Line results revealed that compounds **7c**, **11b**, **11c**, **11e** and **13c** exhibited strong to very strong antitumor activity with IC_{50} values of 9.88, 17.52, 19.24, 13.64, and 10.33 μM, respectively. Compounds **9a** and **13a** showed moderate antitumor effects with IC_{50} values of 25.19 and 23.59 μM, respectively. Regarding the MCF-7 cell line: compound **13c** demonstrated superior activity against MCF-7 cells with an IC_{50} of 2.42 μM, surpassing the positive control doxorubicin (IC_{50} = 4.17 μM). Compounds **7c**, **11b**, **11c**, **11e**, **13a**, and **13d** showed potent anti-breast cancer activity with IC_{50} values of 6.93, 8.39, 9.15, 5.92, 18.63, and 14.21 μM, respectively. Compounds **11f** and **13b** exhibited moderate antitumor activity with IC_{50} values of 22.16 and 27.82 μM, respectively.

2.2.2. Structure–activity relationship (SAR). In this SAR study of novel final target compounds for anticancer activity, the oxadiazole series **13a–e** emerged as the most potent, with compound **13c** showing comparable efficacy to doxorubicin against HCT-116, HeLa, and MCF-7 cell lines (IC_{50} values: 6.1, 10.33, and 2.42 μM, respectively). SAR analysis revealed that electron-withdrawing groups in the *para* position, particularly the nitro group in **13c**, enhanced anticancer potency, while electron-donating substituents decreased activity. TP/1,3,4-thiadiazole-aryl urea hybrids **9a–d** demonstrated weaker cytotoxicity compared to other series. In the piperazine derivatives **7a–e**, compound **7c**, featuring a bulky aromatic group, showed the highest potency. The pyrimidine series **11a–f** exhibited a correlation between the presence of electron-rich groups and

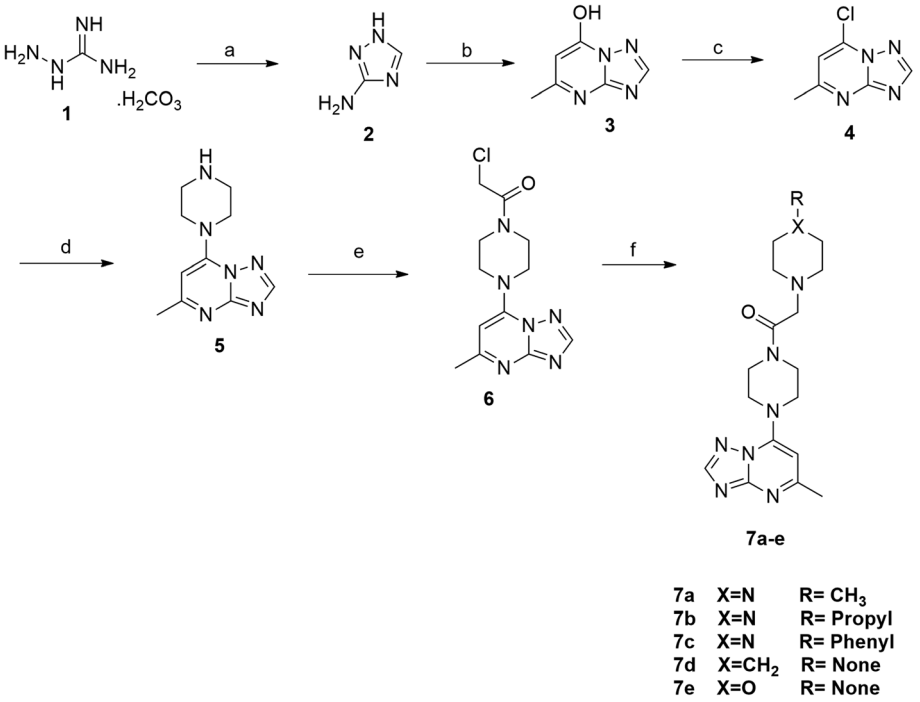

Scheme 1 Reagents and conditions: (a) formic acid, reflux; (b) EAA, acetic acid, reflux; (c) $POCl_3$, reflux; (d) piperazine, K_2CO_3, dioxane, reflux; (e) CAC, TEA, DCM, rt; (f) substituted piperazine, TEA, DCM, reflux.

increased antitumor activity, with compound **11e** (containing dimethoxy groups) being the most active. Conversely, electron-deficient groups in this series led to decreased activity. These findings provide valuable insights into the structural features that influence the anticancer potential of these heterocyclic compounds, potentially guiding future development of more effective anticancer agents.

2.2.3. *In vitro* cytotoxicity towards normal human cells. The cytotoxicity of the newly synthesized compounds was evaluated against the WI-38 normal fibroblast cell line to assess their selectivity towards cancer cells. All tested compounds demonstrated lower toxicity to normal fibroblasts compared to their effects on cancer cell lines, as evidenced by their higher IC_{50} values in WI-38 cells. Notably, the most active compounds against cancer cells **7c**, **11e**, and **13c** exhibited significantly reduced cytotoxicity towards WI-38 cells, with IC_{50} values of 43.93, 60.30, and 38.65 μM, respectively. These results are particularly promising when compared to the reference compound doxorubicin, which showed higher toxicity to normal cells (IC_{50} = 6.72 μM). This favorable selectivity profile

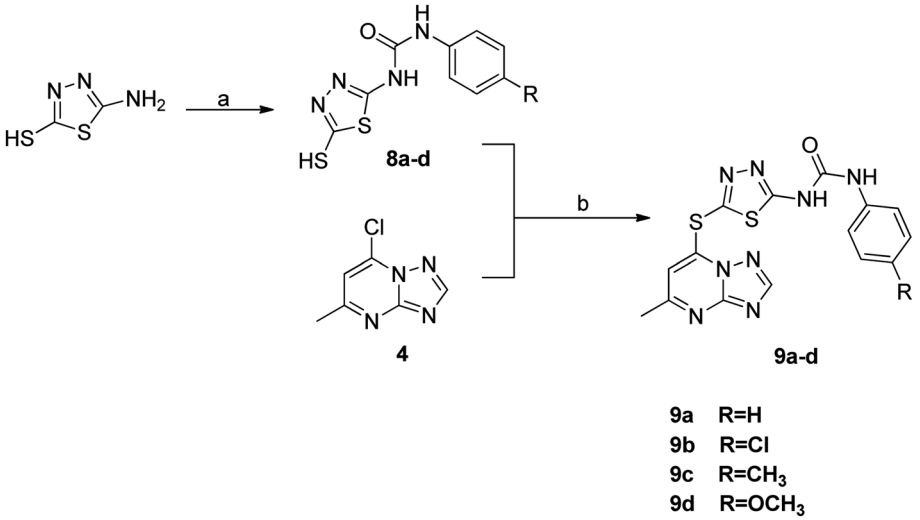

Scheme 2 Reagents and conditions: (a) substituted phenyl isocyanate, acetonitrile, reflux; (b) K_2CO_3, acetone, reflux.

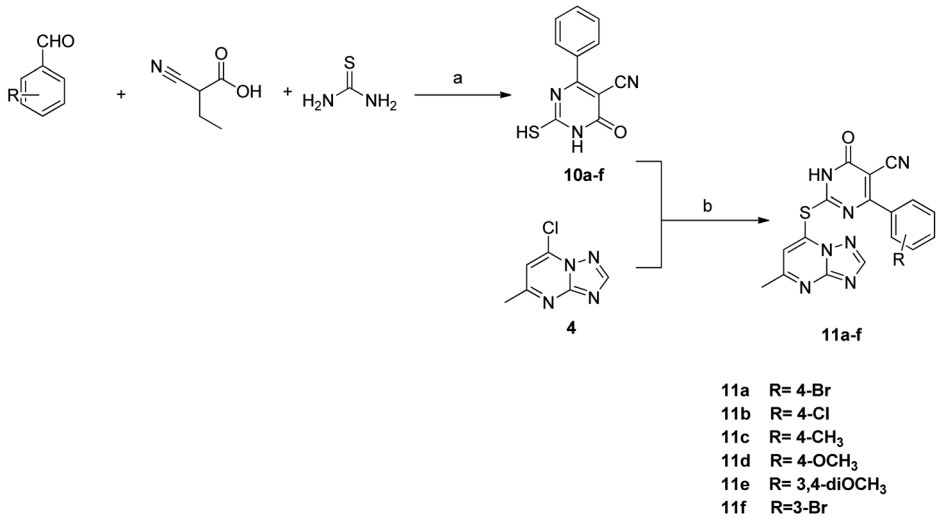

Scheme 3 Reagents and conditions: (a) K_2CO_3, ethanol, reflux; (b) K_2CO_3, acetone, reflux.

suggests that these compounds may have potential as anticancer agents with reduced side effects on normal tissues, warranting further investigation into their mechanism of action and *in vivo* efficacy (Table 1).

2.2.4. EGFR, TOP-II, HER2 and aromatase multitarget enzyme inhibition assay. Comparing compounds **7c**, **11e**, and **13c** to the reference drugs, **13c** stands out with excellent multitarget activity, particularly for EGFR (0.087 μM) and HER-2 (0.078 μM), outperforming lapatinib (0.092 μM for EGFR) and approaching erlotinib's potency for HER-2 (0.032 μM). All three active compounds show broad-spectrum inhibition across EGFR, TOP-II, HER-2, and ARO, with **13c** generally being the most potent. For TOP-II inhibition, the synthesized compounds are comparable to doxorubicin (33.97 μM), with **13c** (31.56 μM) being slightly more potent. While erlotinib and ketoconazole outperform the active compounds for HER-2 and ARO inhibition respectively, the active compounds' multi-target profile, especially **13c**'s, suggests potential advantages in therapeutic applications, possibly offering improved efficacy or reduced drug resistance compared to single-target inhibitors (Table 2).

2.2.5. Cell cycle analysis in MCF-7 breast cancer cell line. Compound **13c**, identified as the most potent anti-breast cancer agent in this study, was further evaluated for its effects on cell cycle progression in MCF-7 breast cancer cells using established procedures. Flow cytometric analysis revealed that **13c** induces cell cycle arrest at the S phase. Quantification of the results demonstrated a significant increase in the S phase cell population from 24.83% in untreated controls to 37.01% in **13c**-treated cells. This S phase arrest suggests that **13c** may interfere with DNA synthesis or repair mechanisms, potentially contributing to its antiproliferative effects. The observed cell cycle perturbation, in conjunction with its apoptosis-inducing properties, provides further insight into the multifaceted anticancer activity of **13c** and strengthens its potential as a promising therapeutic candidate for breast cancer treatment (Fig. 3 and Table 3).

2.2.6. Detection of apoptosis. The development of apoptosis inducers represents a promising therapeutic strategy in the search for potent anticancer drugs. To investigate this potential, the most active compound, **13c**, was evaluated for its ability to induce apoptosis in MCF-7 breast cancer cells using

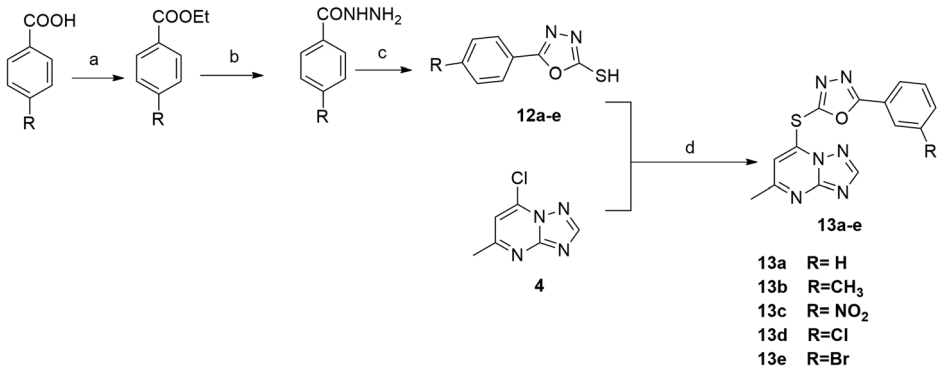

Scheme 4 Reagents and conditions: (a) $C \cdot H_2SO_4$, ethanol, reflux; (b) NH_2NH_2, ethnaol, reflux; (c) CS_2, KOH, ethanol, reflux; (d) K_2CO_3, dioxane, reflux.

Table 1 The activities of the novel compounds over normal cells (WI-38) and 3 cancer cell lines and the values of their IC_{50} (μM) are provided

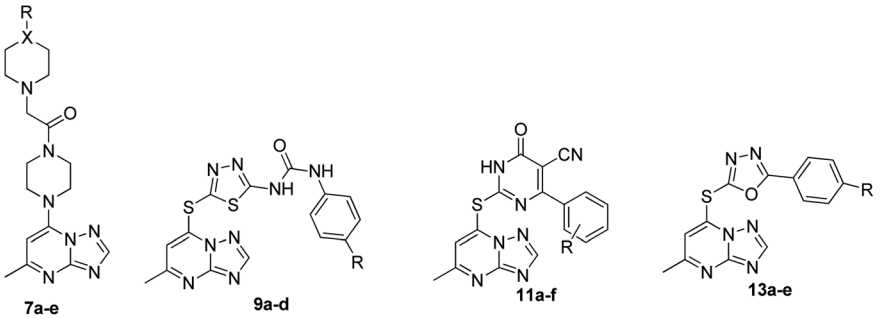

Comp.	R	IC_{50}[a] (μM) HCT-116	HeLa	MCF-7	WI-38
7a	CH_3, X = N	65.80 ± 3.8	52.40 ± 3.4	55.96 ± 3.2	>100
7b	*n*-Propyl, X = N	62.61 ± 3.6	45.71 ± 2.4	53.85 ± 2.8	32.79 ± 2.1
7c	Phenyl, X = N	**7.03 ± 0.6**	**9.88 ± 0.6**	**6.93 ± 0.4**	**43.93 ± 2.4**
7d	None, X = CH_2	73.89 ± 4.2	59.10 ± 3.3	67.34 ± 3.4	36.45 ± 2.0
7e	None, X = O	88.43 ± 4.5	78.54 ± 4.2	84.68 ± 4.1	26.32 ± 1.9
9a	H	44.35 ± 2.6	25.19 ± 2.0	37.21 ± 2.3	48.35 ± 2.6
9b	Cl	>100	87.68 ± 4.4	>100	64.72 ± 3.5
9c	CH_3	58.50 ± 3.3	51.93 ± 2.8	46.05 ± 2.5	18.11 ± 1.3
9d	OCH_3	>100	82.39 ± 4.1	92.38 ± 4.4	>100
11a	4-Br	41.03 ± 2.4	33.41 ± 2.3	30.49 ± 2.1	75.94 ± 4.1
11b	4-Cl	12.61 ± 1.0	17.52 ± 1.4	8.39 ± 0.6	56.23 ± 3.0
11c	4-CH_3	21.51 ± 1.5	19.24 ± 1.6	9.15 ± 0.7	45.03 ± 2.4
11d	4-OCH_3	47.87 ± 2.7	63.42 ± 3.6	34.63 ± 2.3	71.23 ± 3.9
11e	3,4-diOCH_3	**8.89 ± 0.8**	**13.64 ± 1.1**	**5.92 ± 0.3**	**60.30 ± 3.3**
11f	3-Br	31.16 ± 2.2	35.88 ± 2.2	22.16 ± 1.6	77.28 ± 4.3
13a	H	15.03 ± 1.2	23.59 ± 1.9	18.63 ± 1.3	91.39 ± 4.9
13b	CH_3	29.32 ± 2.0	39.01 ± 2.4	27.82 ± 2.0	83.54 ± 4.5
13c	NO_2	**6.10 ± 0.5**	**10.33 ± 0.9**	**2.42 ± 0.1**	**38.65 ± 2.2**
13d	Cl	24.79 ± 1.8	42.92 ± 2.5	14.21 ± 1.1	66.08 ± 3.8
13e	Br	55.07 ± 3.5	57.41 ± 3.2	42.56 ± 2.4	>100
DOX		5.23 ± 0.3	5.57 ± 0.4	4.17 ± 0.2	6.72 ± 0.5

[a] The concentration required to prevent 50% of cancer cells from proliferating is known as the IC_{50} value. The mean ± SD from the dose–response curves of three separate trials is used to illustrate the data. IC_{50}, expressed in μg mL^{-1}, ranges from 1–10 (extremely strong), 11–20 (strong), 21–50 (moderate), and 51–100 (weak).

Table 2 Inhibitory effect of compounds **13c**, **7c** & **11e** against EGFR, TOP-II, HER-2 and aromatase enzymes

Comp.	IC_{50} (μM) EGFR	TOP-II	HER-2	ARO
13c	0.087	31.56	0.078	0.156
7c	0.169	48.48	0.21	0.567
11e	0.246	36.72	0.116	0.38
Lapatinib	0.092			
Erlotenib			0.032	
Doxorubicin		33.97		
Ketoconazole				0.092

Annexin V and PI double staining flow cytometry. Results demonstrated that **13c** treatment led to a significant accumulation of both early and late apoptotic cells compared to the untreated control. Specifically, after 24 hours of treatment, the proportion of total apoptotic cells (early and late) in **13c**-treated MCF-7 cells increased dramatically to 42.13%, in stark contrast to the 2.47% observed in untreated controls. This substantial increase in apoptotic cell population strongly suggests that **13c** exerts its growth inhibitory effects on cancer cells primarily through the induction of apoptosis, underlining its potential as a promising anticancer agent and warranting further investigation into its molecular mechanisms and *in vivo* efficacy (Fig. 4).

2.2.7. *In vivo* anti-breast cancer activity assay of compound 13c and its effect on the apoptotic marker (caspase-3) level. The compelling *in vitro* cytotoxic activity of compound **13c** prompted further investigation of its efficacy *in vivo*. We employed a DMBA-induced breast cancer model to evaluate the compound's antitumor potential. The assessment criteria included body weight changes, tumor volume progression, and histopathological examination, with doxorubicin (DOX) serving as a positive control.[37]

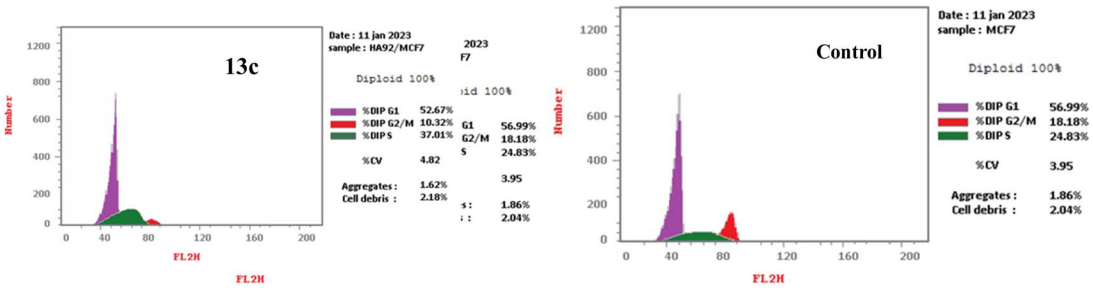

Fig. 3 The DNA ploidy in MCF-7 cells was examined using flow cytometry following treatment with compound **13c**.

Table 3 The impact of **13c** on the distribution of cell cycles in MCF-7 cells, including DMSO as a control

	Cell cycle distribution (%)		
Comp. no.	G0-G1	S	G2-M
13c	52.67	37.01	10.32
Control (DMSO)	56.99	24.83	18.18

Body weight analysis revealed that while the normal control group maintained minimal weight fluctuations, DMBA-treated groups exhibited significant weight gain. Analysis of body weight progression over the 20 days experimental period revealed distinct patterns among the groups. The control group exhibited a steady, moderate increase from 20.51 g to 28.91 g, representing typical growth. In contrast, the DMBA group, starting with the lowest initial weight (18.8 g), demonstrated the most pronounced weight gain, reaching 35.2 g by day 20, significantly surpassing the control. The **13c**-treated group, beginning at a weight comparable to the control (20.2 g), showed a more moderate increase, attaining 30.6 g by the study's conclusion. This pattern suggests **13c**'s potential to mitigate DMBA-induced weight changes. The DOX group, while still exceeding the control's final weight, exhibited a weight gain pattern (19.8 g to 31.8 g) intermediate between the control and DMBA groups. Notably, both **13c** and DOX treatments appeared to moderate the excessive weight gain observed in the untreated DMBA group, with **13c** demonstrating a slightly more favorable effect in maintaining body weight closer to control levels, particularly in the latter stages of the experiment (Fig. 5a).

Tumor volume measurements provided crucial insights into treatment efficacy. The untreated DMBA group demonstrated exponential tumor growth, with volumes reaching approximately 2.4 mm^3 by day 20. In contrast, the **13c**-treated group showed a significantly moderated growth pattern, with final tumor volumes of about 0.9 mm^3, representing a substantial 62.5% reduction compared to the untreated group. This reduction was comparable to the effect observed in the positive control group treated with DOX, which achieved a 75% reduction in final tumor volume (approximately 0.6 mm^3) relative to the DMBA control.

These findings corroborate the *in vitro* cytotoxicity results, indicating that **13c** possesses significant tumor-suppressive properties *in vivo*. **13c** demonstrated a remarkable ability to inhibit tumor growth, with efficacy approaching that of the established chemotherapeutic agent used as a positive control. This promising performance warrants further investigation of **13c** as a potential anticancer agent (Fig. 5b).

The histopathological analysis (Fig. 6A) reveals striking differences across the treatment groups. The control group exhibits normal mammary gland structure with ducts lined by a single, well-organized epithelium. In contrast, the DMBA group shows severe pathological changes, including extensive fibrosis, significant leukocyte infiltration, and marked epithelial disorganization characterized by atypical hyperplasia and increased mitotic figures. The **13c**-treated group demonstrates notable improvement over the DMBA group, presenting only mild periductal fibrosis and limited leukocyte infiltration, though some abnormalities persist. Still, it was comparable to

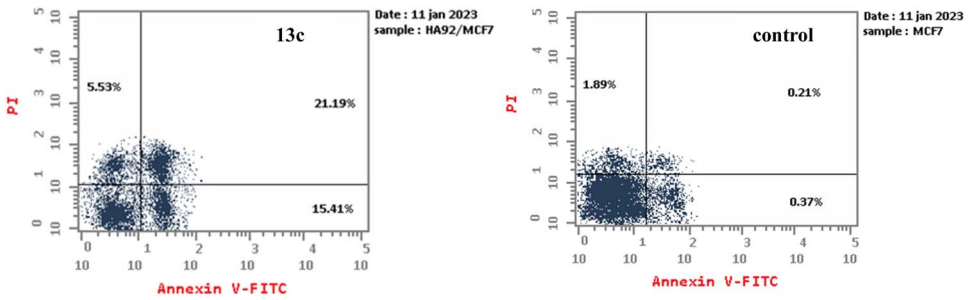

Fig. 4 Impact of compound **13c** on the percentage of Annexin V-FITC positive staining in MCF-7 cells after 24 hours of incubation, with DMSO used as a control. The four stages of cell death are Q1, necrotic cells; Q2, late apoptosis; Q3, living cells; and Q4, early apoptosis.

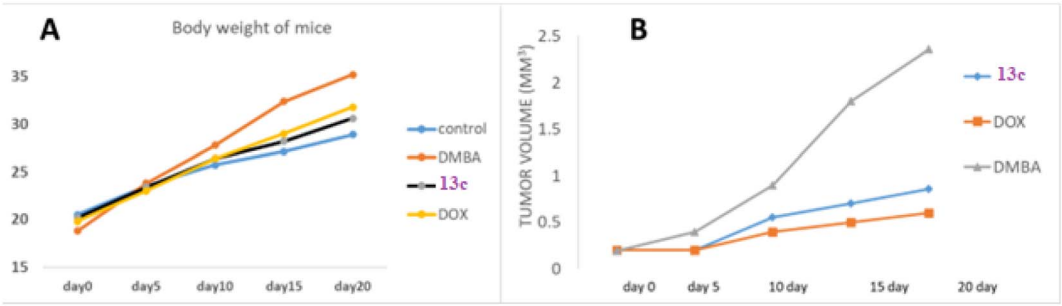

Fig. 5 (A) Body weight changes in mice over 20 days following tumor induction with 7,12-dimethylbenz[*a*]anthracene (DMBA). Groups include control (untreated), DMBA-only, **13c**-treated, and doxorubicin (Dox)-treated mice. (B) Tumor volume progression in the same groups over 20 days. Data represents mean values for each group, illustrating the impact of **13c** and Dox on body weight and tumor growth in mouse model.

the Dox-treated group that exhibited only mild inflammation and largely normalized epithelial ducts.

Interestingly, immunohistochemical analysis for caspase-3 (Fig. 6B) gave insights into the apoptotic activity across groups. The control group displays baseline positive staining in ductal epithelial cells, indicating normal apoptotic function. The DMBA group, however, shows negatively stained ductal epithelial cells, suggesting a severe suppression of apoptosis – a hallmark of cancer progression. The **13c**-treated group shows a marked increase in positively stained cells compared to the DMBA group, indicating a partial restoration of apoptotic function which resembles the profile of Dox-treated group.

Quantitative analysis of caspase-3 expression (Fig. 6C) further elucidates these findings. The control group shows 4.5 ± 0.2 caspase-3 positive cells. On the other hand, the DMBA group exhibited a drastic 89% decrease to 0.5 ± 0.1 cells, underscoring the severe suppression of apoptosis in cancer cells. The Dox-treated group demonstrates remarkable efficacy, with 4.0 ± 0.2 cells, representing a 700% increase from the DMBA group and only an 11% decrease from the control. The **13c**-treated group shows significant improvement with 2.3 ± 0.3 cells, a 360% increase from the DMBA group.

These results collectively indicate that **13c** significantly enhances apoptotic activity in DMBA-induced mammary gland cancer, achieving about 51% of the control's apoptotic activity. Hence, its ability to normalize tissue morphology and significant increasement could be attributed to the increase in caspase-3 activity observed with **13c**. Also, the inhibition of several key molecular targets involved in cancer cell survival and proliferation. Inhibition of EGFR (Epidermal Growth Factor

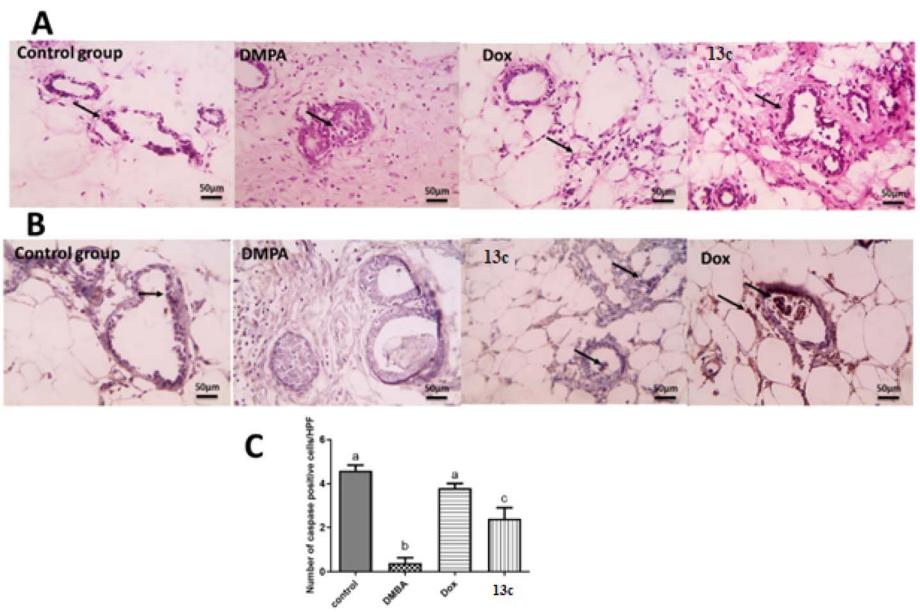

Fig. 6 (A) HE-stained sections: the control group shows normal ducts with organized epithelium (black arrows). The DMBA group exhibits disorganized ductal cells with atypical hyperplasia (black arrows). The **13c**-treated group shows mild fibrosis with few leukocytes (black arrows), while the Dox-treated group shows mild inflammation and normalized ducts (black arrow). (B) Caspase-3 immunostaining: the control group has positive ductal epithelial cells (black arrows); the DMBA group is mostly negative. The **13c**-treated group has fewer positive cells (black arrows) than the Dox-treated group (black arrow). IHC counterstained with Mayer's hematoxylin. (C) Bar charts show a significant decrease in positive cells in the DMBA group and a significant increase in the Dox and **13c** groups ($P < 0.05$).

Table 4 The binding energy of the most active compounds in comparison to the co-crystallized ligand for each prospective target

No.	Compound	EGFR	HER-2	TOP-II	Aromatase
1	**13c**	−8.0	−10.4	−10.7	−9.9
2	**11e**	−7.9	−8.9	−9.5	−9.1
3	**7c**	−7.7	−10.3	−10.2	−10.6
4	Co-crystallized ligand in EGFR	−8.1	—	—	—
5	Co-crystallized ligand in HER-2	—	−11.6	—	—
6	Co-crystallized ligand in Top-II	—	—	−10.9	—
7	Co-crystallized ligand in aromatase	—	—	—	−10.7

Receptor) and HER2 (Human Epidermal Growth Factor Receptor 2) can lead to decreased activation of pro-survival signaling pathways, making cells more susceptible to apoptosis. Aromatase inhibition in hormone-dependent breast cancers can reduce estrogen production, potentially sensitizing cells to apoptotic stimuli. TOP-II inhibition can induce DNA damage, triggering the intrinsic apoptotic pathway. The observed increase in caspase-3 activity with **13c** treatment could therefore be a downstream effect of inhibiting one or more of these targets.

2.3. Molecular docking

Since compounds **13c**, and **11e** and **7c** showed promising inhibitory activity against enzymes under the study, we utilized molecular docking to explain their binding mode. Firstly, the evaluation of their binding energy in comparison to co-crystallized ligand revealed the better activity of **13c** over other compounds as shown in Table 4. Hence its molecular interaction with the targeted enzyme was further investigated.

In the case of EGFR enzyme, compound **13c** with TP core appears to be a central anchor, forming hydrogen bonds with LEU A:799 and ASP A:800, which are critical for positioning the

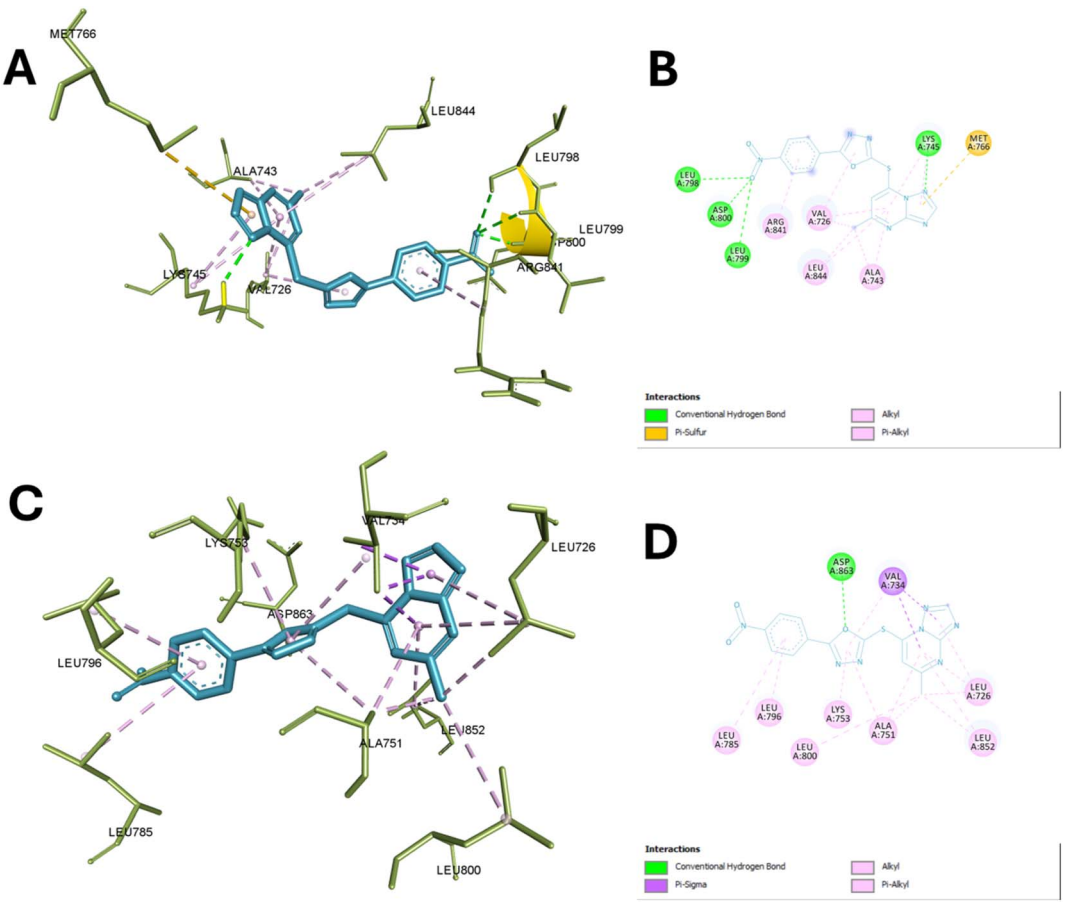

Fig. 7 Binding of compound **13c** with the active sites of EGFR and HER-2. (A) and (B) Show the 3D and 2D interactions of **13c** with the active site of EGFR (PDB ID: 4WKQ), respectively, highlighting hydrogen bonds, hydrophobic contacts, and ionic interactions. (C) and (D) Illustrate the 3D and 2D interactions of **13c** with the active site of HER-2 (PDB ID: 3PP0), emphasizing similar key interactions within the active site pockets.

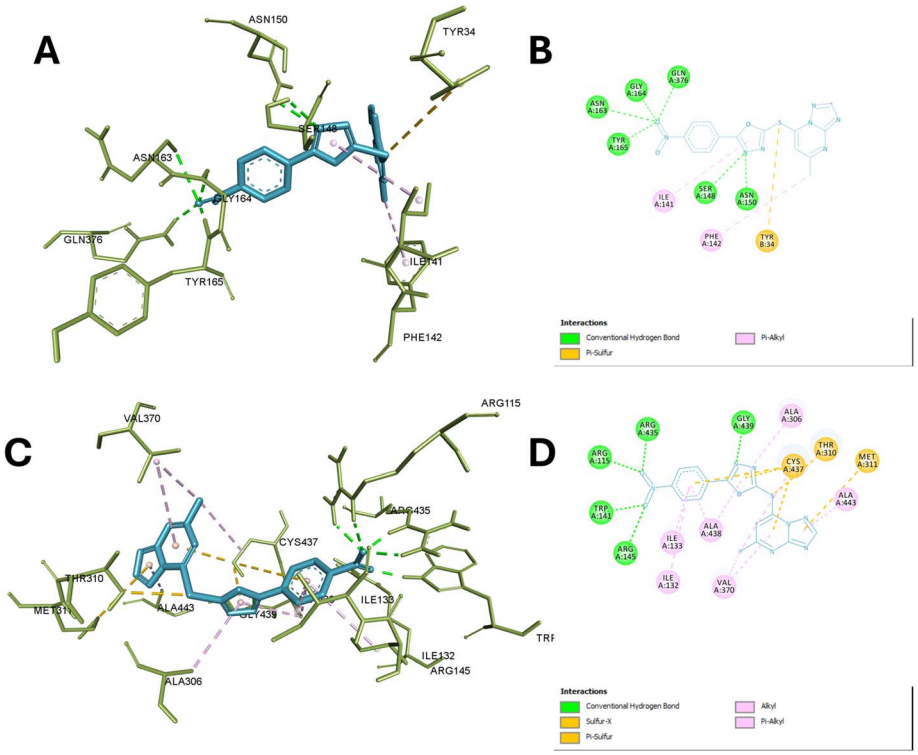

Fig. 8 Interaction of compound **13c** with aromatase and TOP-II. (A) and (B) Display the 3D and 2D interactions of **13c** with the active site of TOP-II (PDB ID: 1ZXM), respectively, detailing hydrogen bonds, hydrophobic contacts. (C) and (D) Present the 3D and 2D interactions of **13c** with the active site of aromatase (PDB ID: 3S79), highlighting the key binding interactions, including hydrogen bonds, and hydrophobic interactions.

ligand within the active site. This interaction contributes significantly to the compound's binding affinity and specificity for EGFR. The 2-mercapto oxadiazole portion of the molecule seems to engage in hydrophobic interactions with VAL A:726 and potentially contributes to the interaction with MET A:766, which could be a pi-stacking interaction.

This interaction with the methionine gatekeeper residue is particularly noteworthy as it often plays a crucial role in inhibitor selectivity. The nitrophenyl group, extending from the core structure, appears to form hydrophobic contacts with LEU A:844 and ALA A:743, further stabilizing the ligand's position. Additionally, this group may be involved in the hydrogen bonding interaction observed with LEU A:798. The compound's ability to engage multiple residues through its diverse functional groups suggests a potentially high affinity and specificity for EGFR.

Moreover, compound **13c** also showed significant interaction with the active site of HER-2. A key hydrogen bond is formed between the ligand and ASP A:863. This interaction is complemented by an extensive network of hydrophobic contacts involving residues VAL A:734, LEU A:726, LEU A:852, ALA A:751, LYS A:753, LEU A:800, LEU A:785, and LEU A:796. The triazole moiety seems centrally positioned, possibly engaging with ASP A:863, while the pyrimidine-like structure orients towards VAL A:734 and LEU A:726, suggesting that these interactions may be crucial for binding stability.

Notably, the nitrophenyl group extends into a hydrophobic pocket formed by leucine residues, indicating a snug fit within the active site. This binding profile, with its combination of specific hydrogen bonding and extensive hydrophobic interactions, suggests that the compound could be a potent HER-2 inhibitor. The involvement of residues like VAL A:734 and LEU A:726, potentially part of the ATP-binding region, further emphasizes the ability of the compound to exert good inhibitory activity as shown in the experimental enzyme assay. Fig. 7 illustrates the binding of compound **13c** with the active site of EGFR and HER-2.

The molecular docking study of **13c** with the active site of TOP-II reveals a detailed interaction profile that is crucial for understanding its inhibitory potential. The compound establishes several hydrogen bonds, hydrophobic interactions, and π–π stacking interactions with key amino acid residues within the active site. Specifically, the 2-mercapto oxadiazole moiety formed 2 hydrogen bonds with ASN A:150 and SER A:148, ensuring a stable orientation and strong interaction within the enzyme's active site.

Additionally, it formed hydrophobic interaction with Ile A:141 while, the TP ring also participates in significant π–π stacking interactions with PHE A:142 and TYR B:34, enhancing the binding affinity and stabilization of the compound within the active site. Nitro phenyl fragments were able to interact efficiently with several residues through hydrogen bonding such as Asn A:163, Tyr A:165, Gly A:164, and Gln A:376, further contributing to the compound's binding stability. Hydrophobic interactions are observed with ILE A:141 and, with the latter also involved in π–π stacking with the aromatic ring of the

compound, underscoring the combined role of hydrophobic and aromatic interactions in reinforcing the compound's affinity for the enzyme.

These interactions collectively ensure high binding affinity, specificity, and stability, underscoring the compound's potential as a potent enzyme inhibitor by effectively occupying the active site. Specifically, the involvement of these amino acids in the catalytic activity of TOP-II highlights their significance. Asn A:163 and Asn A:150 are essential for stabilizing the DNA cleavage complex, and their interaction with the compound could inhibit this stabilization.

Tyr A:165 and Tyr B:34 are crucial for forming a covalent bond with the DNA phosphate backbone during the cleavage and rejoining process, and their interaction with the compound could block their activity. Gly A:164 and Gln A:376 provide flexibility and stabilization to the active site, and their interaction with the compound could hinder these roles. Ser A:148 is involved in ATP hydrolysis, and its interaction with the compound could disrupt this critical step. Lastly, Ile A:141 and Phe A:142 are important for maintaining the structural integrity of the active site, and their interaction with the compound could alter the enzyme's conformation. Thus, the compound's binding to these key residues effectively inhibits the catalytic activity of Topo II, making it a potent enzyme inhibitor.[38]

Finally, molecular docking of **13c** in the active site of aromatase reveals significant interactions with the active site of aromatase. The nitro group forms conventional hydrogen bonds with ARG A:115, ARG A:145, TRP A:141, and ARG A:435 anchoring this portion of the molecule in the binding pocket. The phenyl group engages in pi–alkyl interactions with ILE A:133, ILE A:133 and ALA A:438. While TP scaffold interacts through pi-sulfur bonds with CYS A:437, THR A:310, and MET A:311 and hydrophobic interaction with ALA A:443 and VAL A:370. A conventional hydrogen bond is also observed between GLY A:439 and the 2-mercapto oxadiazole moiety.

Moreover, it also showed hydrophobic interaction with ALA A:306 and ALA A:438. These interactions collectively contribute to the compound's stability within the aromatase active site. The observed interactions involve several residues crucial for aromatase function. ARG A:115 and ARG A:145 are part of the substrate access channel and play a role in substrate recognition and positioning. TRP A:141 is involved in maintaining the structural integrity of the active site. CYS A:437 is a key residue in the catalytic mechanism, participating in the electron transfer process during substrate oxidation.

The interactions with ILE A:133, ALA A:438, and VAL A:370 are to contribute to defining the hydrophobic environment necessary for optimal substrate binding and orientation. GLY A:439 is a part of the conserved glycine-rich loop that is important for cofactor binding and positioning. Hence, this interactions suggests that this compound may effectively occupy the aromatase active site, potentially interfering with substrate binding and catalysis supporting the experimental findings in the enzyme inhibition assays,[39,40] Fig. 8 depict the interaction of compound **13c** with aromatase and TOP-II.

3. Conclusion

New series of TP compounds **7a–e**, **9a–d**, **11a–f** and **13a–e** were synthesized. The structure of the novel hybrids was confirmed using different spectroscopic techniques. They were assessed for their cytotoxic effect *vs.* three cancer cell lines: HCT116, HeLa & MCF7. **13c** showed the best antitumor activity of the tested compounds with IC_{50} 6.10, 10.33 and 2.42 μM in succession. In addition, compound **11e** revealed a potent anticancer effect against HCT116 and MCF-7 with IC_{50} 8.89 & 5.92 μM, respectively. Also, compound **7c** exhibited very strong activity against HCT116, HeLa & MCF7 with IC_{50} 7.03, 9.88 and 6.93, respectively. The most potent cytotoxic compounds were tested in a multi-target suppressive test, and **13c** had the highest inhibition against EGFR, TOP-II, HER2, and ARO with an IC_{50} of 0.087, 31.56, 0.078 and 0.156 μM, respectively. According to flow cytometric testing, the most effective multi-target inhibitory agent, **13c**, was shown to suppress the cell cycle in the S phase in the MCF-7. The compelling *in vitro* cytotoxic activity of compound **13c** prompted further investigation of its efficacy *in vivo*. **13c** demonstrated a remarkable ability to inhibit tumor growth, with efficacy approaching that of the established chemotherapeutic agent used as a positive control. The histopathological analysis reveals **13c**-treated group demonstrating notable improvement over the DMBA group, presenting only mild periductal fibrosis and limited leukocyte infiltration. Confirmation of the obtained results was done with the aid of the docking study, which showed that the three motifs might adhere to the enzyme's major active sites, and the results were in good accordance with the experimental inhibitory results.

4. Experimental

4.1. Chemistry

All melting points (°C) were recorded on Stuart melting point apparatus (SMP 30) and are uncorrected. ^{1}H-NMR and ^{13}C-NMR spectra were performed in (DMSO-d_6 or $CDCl_3$) at ^{1}HNMR (400 MHz), ^{13}CNMR (100 MHz) using an NMR spectrometer (δ ppm), NMR Unit, Faculty of Pharmacy, Mansoura University, using TMS as an internal standard. The following are the abbreviations: (s) for singlet; (d) for doublet; (t) for triplet; (m) for multiplet; and (br) for broad. At Al-Azhar University in Egypt's Regional Center for Mycology and Biotechnology (RCMB), mass spectra were conducted using a Thermo Scientific GCMS type ISQ. For the C, H, and N elements, microanalyses were performed at Cairo University using a PerkinElmer 240 elemental analyzer. The results were obtained within an acceptable range of theoretical values. With a UV lamp set at 254 nm, compounds were found. Every chemical and reagent that was utilized was bought from commercial sources including Aldrich Chemicals Co. in the United States. The key precursor compound **4** and intermediate compounds **8a–d**, **10a–f**, **12a–e** were prepared according to reported procedures in literature.[35,36,41]

4.1.1. General procedure for the preparation of 2-chloro-1-(4-(5-methyl-[1,2,4]triazolo[1,5-*a*]pyrimidin-7-yl)piperazin-1-yl) ethanone (6). To a mixture of compound **5** (100 mg, 0.46

mmole) and triethylamine (2 eq.) in dichloromethane, chloro acetyl chloride (1 eq.) was introduced and mixed at room temperature for 3 hours. Following the completion of the reaction, the reaction mixture was placed on ice and methylene chloride was used to extract it. The organic layer was dried using sodium sulphate and evaporated to afford yellow oil (81.4 mg, 61% yield).

4.1.2. General procedure for the preparation of piperazine derivatives (7a–e). To a solution of piperazine derivative in methylene chloride (4 mL) and triethylamine (2 eq.) were added at rt. Compound **6** (0.1 g, 0.9819 mmol) was added to the resulting mixture and heated to reflux. When TLC showed that the reaction was finished, the methylene chloride was evaporated *in vacuo*. A 20 mL solution was used to dilute the residue that was obtained. The reaction mixture was extracted using 3 × 5 mL of CH_2Cl_2. After being gathered, the organic layers were dried over anhydrous $MgSO_4$, cleaned with saturated brine solution, and concentrated in a vacuum. Column chromatography was used to purify the resulting crude.

*4.1.2.1 1-(4-(5-Methyl-[1,2,4]triazolo[1,5-a]pyrimidin-7-yl) piperazin-1-yl)-2-(4-methylpiperazin-1-yl)ethenone (**7a**).* White solid; (0.09 g, 74%). M. p. 160–162 °C. ^{1}H NMR (400 MHz, DMSO-d_6) δ 8.50 (s, 1H), 6.67 (s, 1H), 3.91 (d, J = 4.2 Hz, 2H), 3.84 (d, J = 3.9 Hz, 4H), 3.75–3.69 (m, 2H), 3.24 (s, 2H), 2.55 (s, 3H), 2.51–2.27 (m, 8H), 2.23–2.18 (m, 3H). ^{13}C NMR (101 MHz, DMSO-d_6) δ 168.4, 164.9, 154.3, 149.9, 95.4, 61.1, 55.0, 52.7, 48.4, 47.90, 46.1, 25.0. GC-MS EI m/z (%): 358.34 (M^+, 18.22). Anal. calcd for $C_{17}H_{26}N_8O$ (358.22): C, 56.96; H, 7.31; N, 31.26. Found: C, 56.88; H, 7.26; N, 31.29%.

*4.1.2.2 1-(4-(5-Methyl-[1,2,4]triazolo[1,5-a]pyrimidin-7-yl) piperazin-1-yl)-2-(4-propylpiperazin-1-yl)ethenone (**7b**).* White solid; (0.1 g, 76%). M. p. 145–147 °C. ^{1}H NMR (400 MHz, $CDCl_3$) δ 8.22 (s, 1H), 6.09 (s, 1H), 3.86–3.76 (m, 4H), 3.69–3.50 (m, 4H), 3.23 (s, 2H), 2.74–2.68 (m, 4H), 2.51 (s, 3H), 2.50–2.42 (m, 4H), 2.38–2.28 (m, 2H), 1.55–1.44 (m, 2H), 0.86 (t, J = 7.3 Hz, 3H). ^{13}C NMR (101 MHz, $CDCl_3$) δ 166.2, 163.9, 156.2, 153.2, 149.1, 93.6, 59.4, 59.2, 52.3, 51.4, 46.9, 43.9, 24.2, 18.4, 10.7. GC-MS EI m/z (%): 386.39 (M^+, 26.22). Anal. calcd for $C_{19}H_{30}N_8O$ (386.25): C, 59.04; H, 7.82; N, 28.99. Found: C, 59.08; H, 7.72; N, 28.91%.

*4.1.2.3 1-(4-(5-Methyl-[1,2,4]triazolo[1,5-a]pyrimidin-7-yl) piperazin-1-yl)-2-(4-phenylpiperazin-1-yl)ethenone (**7c**).* White solid; (0.091 g, 68%). M. p. 190–192 °C. ^{1}H NMR (400 MHz, $CDCl_3$) δ 8.24 (s, 1H), 7.23 (t, J = 7.9 Hz, 2H), 6.86 (t, J = 9.0 Hz, 3H), 6.10 (s, 1H), 3.86 (s, 4H), 3.78–3.66 (m, 4H), 3.43 (s, 2H), 3.17–3.06 (m, 4H), 2.92 (s, 4H), 2.52 (s, 3H). ^{13}C NMR (101 MHz, $CDCl_3$) δ 164.0, 156.1, 153.3, 149.7, 149.0, 148.9, 128.3, 119.8, 115.7, 93.8, 51.1, 49.0, 46.4, 44.4, 40.7, 24.2. GC-MS EI m/z (%): 420.19 (M^+, 22.25). Anal. calcd for $C_{22}H_{28}N_8O$ (420.24): C, 62.84; H, 6.71; N, 26.65. Found: C, 62.75; H, 6.70; N, 26.57%.

*4.1.2.4 1-(4-(5-Methyl-[1,2,4]triazolo[1,5-a]pyrimidin-7-yl) piperazin-1-yl)-2-(piperidin-1-yl)ethenone (**7d**).* White solid; (0.099 g, 85%). M. p. 185–187 °C. ^{1}H NMR (400 MHz, $CDCl_3$) δ 8.22 (s, 1H), 6.09 (s, 1H), 3.80 (s, 4H), 3.53–3.46 (m, 2H), 3.46–3.37 (m, 2H), 3.21 (s, 2H), 2.71 (d, J = 4.2 Hz, 4H), 2.51 (s, 3H), 1.59 (d, J = 4.7 Hz, 2H), 1.50 (dd, J = 10.8, 4.9 Hz, 4H). ^{13}C NMR (101 MHz, $CDCl_3$) δ 167.0, 164.8, 157.2, 154.1, 150.2, 94.6, 60.4, 52.5, 47.9, 46.6, 26.6, 25.2, 24.4. GC-MS EI m/z (%): 343.28 (M^+, 26.11). Anal. calcd for $C_{17}H_{25}N_7O$ (343.21): C, 59.45; H, 7.34; N, 28.55. Found: C, 59.36; H, 7.30; N, 28.59%.

*4.1.2.5 1-(4-(5-Methyl-[1,2,4]triazolo[1,5-a]pyrimidin-7-yl) piperazin-1-yl)-2-morpholinoethanone (**7e**).* White solid; (0.095 g, 81%). M. p. 164–166 °C. ^{1}H NMR (400 MHz, DMSO-d_6) δ 8.45 (s, 1H), 6.63 (s, 1H), 3.99–3.67 (m, 8H), 3.64–3.51 (m, 8H), 3.22 (s, 2H), 2.43 (s, 3H). ^{13}C NMR (101 MHz, DMSO-d_6) δ 167.9, 164.7, 157.1, 154.4, 145.0, 95.4, 66.6, 61.3, 53.4, 48.4, 45.0, 25.1. GC-MS EI m/z (%): 345.36 (M^+, 19.52). Anal. calcd for $C_{16}H_{23}N_7O_2$ (345.19): C, 55.64; H, 6.71; N, 28.39. Found: C, 55.49; H, 6.75; N, 28.47%.

4.1.3. General procedure for the preparation of 5-((5-methyl-[1,2,4]triazolo[1,5-*a*]pyrimidin-7-yl)thio)-1,3,4-thiadiazol-2-amine (9a–d). Thiol **8a–d** (0.3 mmole) with K_2CO_3 (2 eq) in acetone were stirred at rt for 30 min. Then, the corresponding chloride **4** (0.3 mmole) was added. The resulting mixture was refluxed overnight. The reaction mixture was poured into crushed ice, then acetic acid was added till precipitate, the solid precipitated was filtered and washed with water.

*4.1.3.1 1-(5-((5-Methyl-[1,2,4]triazolo[1,5-a]pyrimidin-7-yl) thio)-1,3,4-thiadiazol-2-yl)-3-phenylurea (**9a**).* White solid; (0.082 g, 72%). M. p. 202–204 °C. ^{1}H NMR (400 MHz, DMSO-d_6) δ 11.57 (s, 1H), 9.26 (s, 1H), 8.69 (s, 1H), 7.52 (d, J = 7.9 Hz, 2H), 7.36 (t, J = 7.9 Hz, 2H), 7.10 (t, J = 7.4 Hz, 1H), 6.85 (s, 1H), 2.55 (s, 3H). ^{13}C NMR (101 MHz, DMSO-d_6) δ 185.8, 165.8, 165.1, 155.9, 154.6, 147.1, 145.9, 138.5, 129.5, 123.9, 119.6, 108.6, 25.2. GC-MS EI m/z (%): 384.15 (M^+, 23.05). Anal. calcd for $C_{15}H_{12}N_8OS_2$ (384.06): C, 46.86; H, 3.15; N, 29.15. Found: C, 46.78; H, 3.11; N, 29.19%.

*4.1.3.2 1-(4-Chlorophenyl)-3-(5-((5-methyl-[1,2,4]triazolo[1,5-a]pyrimidin-7-yl)thio)-1,3,4-thiadiazol-2-yl)urea (**9b**).* White solid; (0.09 g, 71%). M. p. 209–211 °C. ^{1}H NMR (400 MHz, DMSO-d_6) δ 11.66 (s, 1H), 9.35 (s, 1H), 8.69 (s, 1H), 7.56 (d, J = 8.6 Hz, 2H), 7.41 (d, J = 8.6 Hz, 2H), 6.86 (s, 1H), 2.56 (s, 3H). ^{13}C NMR (101 MHz, DMSO-d_6) δ 185.8, 165.3, 165.0, 155.8, 154.6, 147.1, 145.9, 138.4, 131.9, 125.3, 123.1, 108.8, 25.2. GC-MS EI m/z (%): 418.25 (M^+, 18.21). Anal. calcd for $C_{15}H_{11}ClN_8OS_2$ (418.02): C, 43.01; H, 2.65; N, 26.75. Found: C, 43.08; H, 2.51; N, 26.78%.

*4.1.3.3 1-(5-((5-Methyl-[1,2,4]triazolo[1,5-a]pyrimidin-7-yl) thio)-1,3,4-thiadiazol-2-yl)-3-(p-tolyl)urea (**9c**).* White solid; (0.099 g, 83%). M. p. 195–197 °C. ^{1}H NMR (400 MHz, DMSO-d_6) δ 11.51 (s, 1H), 9.08 (s, 1H), 8.69 (s, 1H), 7.39 (d, J = 8.1 Hz, 2H), 7.15 (d, J = 8.1 Hz, 2H), 6.85 (s, 1H), 2.55 (s, 3H), 2.27 (s, 3H). ^{13}C NMR (101 MHz, DMSO-d_6) δ 183.9, 165.7, 165.1, 155.9, 154.6, 147.1, 145.9, 135.8, 133.0, 129.9, 119.7, 108.5, 25.2, 20.9. GC-MS EI m/z (%): 397.92 (M^+, 25.22). Anal. calcd for $C_{16}H_{14}N_8OS_2$ (398.07): C, 48.23; H, 3.54; N, 28.12. Found: C, 48.22; H, 3.66; N, 28.17%.

*4.1.3.4 1-(4-Methoxyphenyl)-3-(5-((5-methyl-[1,2,4]triazolo [1,5-a]pyrimidin-7-yl)thio)-1,3,4-thiadiazol-2-yl)urea (**9d**).* White solid; (0.08 g, 65%). M. p. 201–203 °C. ^{1}H NMR (400 MHz, DMSO-d_6) δ 11.54 (s, 1H), 9.01 (s, 1H), 8.69 (s, 1H), 7.41 (d, J = 7.9 Hz, 2H), 6.92 (d, J = 6.7 Hz, 2H), 6.84 (s, 1H), 3.74 (s, 3H), 2.55 (s, 3H). ^{13}C NMR (101 MHz, DMSO-d_6) δ 187.6, 165.8, 165.1, 156.0, 155.9, 154.6, 147.2, 145.8, 131.3, 121.6, 114.6, 108.5, 55.7, 25.2. GC-MS EI m/z (%): 414.12 (M^+, 19.45). Anal. calcd for

$C_{16}H_{14}N_8O_2S_2$ (414.07): C, 46.37; H, 3.40; N, 27.04. Found: C, 46.25; H, 3.46; N, 27.09%.

4.1.4 General procedure for the preparation of cyano pyrimidine derivatives (11a–f). Appropriate thiol derivatives **10a–e** (0.05 mmole) with K_2CO_3 (2 eq.) in acetone were stirred at rt for 30 min. Then, the corresponding chloride (1.2 eq.) was added. The resulting mixture was refluxed overnight. The precipitated solid was filtered, washed with acetone, and dried to afford the target compound.

*4.1.4.1 4-(4-Bromophenyl)-2-((5-methyl-[1,2,4]triazolo[1,5-a] pyrimidin-7-yl)thio)-6-oxo-1,6-dihydropyrimidine-5-carbonitrile (**11a**).* White solid; (0.094 g, 71%). M. p. 229–231 °C. ^{1}H NMR (400 MHz, DMSO-d_6) δ 8.60 (s, 1H), 8.05 (s, 1H), 7.68 (d, J = 8.6 Hz, 2H), 7.61 (d, J = 8.6 Hz, 2H), 2.66 (s, 3H). ^{13}C NMR (101 MHz, DMSO-d_6) δ 170.1, 167.6, 166.7, 164.6, 155.3, 154.9, 143.3, 136.5, 131.7, 130.5, 124.2, 119.5, 115.3, 91.7, 25.2. GC-MS EI m/z (%): 439.15 (M^+, 24.19). Anal. calcd for $C_{17}H_{10}BrN_7OS$ (438.99): C, 46.38; H, 2.29; N, 22.27. Found: C, 46.22; H, 2.28; N, 22.31%.

*4.1.4.2 4-(4-Chlorophenyl)-2-((5-methyl-[1,2,4]triazolo[1,5-a] pyrimidin-7-yl)thio)-6-oxo-1,6-dihydropyrimidine-5-carbonitrile (**11b**).* White solid; (0.088 g, 74%). M. p. 235–237 °C. ^{1}H NMR (400 MHz, DMSO-d_6) δ 8.60 (s, 1H), 8.05 (s, 1H), 7.68 (d, J = 8.5 Hz, 2H), 7.54 (d, J = 8.5 Hz, 2H), 2.66 (s, 3H). ^{13}C NMR (101 MHz, DMSO-d_6) δ 170.1, 167.6, 166.7, 164.6, 155.3, 154.9, 143.3, 136.2, 135.4, 130.3, 128.8, 119.5, 115.3, 91.7, 25.2. GC-MS EI m/z (%): 395.25 (M^+, 26.28). Anal. calcd for $C_{17}H_{10}ClN_7OS$ (395.04): C, 51.58; H, 2.55; N, 24.77. Found: C, 51.44; H, 2.59; N, 24.63%.

*4.1.4.3 2-((5-Methyl-[1,2,4]triazolo[1,5-a]pyrimidin-7-yl)thio)-6-oxo-4-(p-tolyl)-1,6-dihydropyrimidine-5-carbonitrile (**11c**).* White solid; (0.095 g, 84%). M. p. 220–222 °C. ^{1}H NMR (400 MHz, DMSO-d_6) δ 8.60 (s, 1H), 8.08 (s, 1H), 7.54 (d, J = 8.0 Hz, 2H), 7.25 (d, J = 8.0 Hz, 2H), 2.65 (s, 3H), 2.35 (s, 3H). ^{13}C NMR (101 MHz, DMSO-d_6) δ 170.5, 167.7, 167.5, 164.5, 155.3, 154.9, 143.5, 140.4, 134.6, 129.2, 128.4, 119.8, 115.2, 91.4, 25.1, 21.4. GC-MS EI m/z (%): 375.14 (M^+, 17.65). Anal. calcd for $C_{18}H_{13}N_7OS$ (375.09): C, 57.59; H, 3.49; N, 26.12. Found: C, 57.41; H, 3.55; N, 26.03%.

*4.1.4.4 4-(4-Methoxyphenyl)-2-((5-methyl-[1,2,4]triazolo[1,5-a]pyrimidin-7-yl)thio)-6-oxo-1,6-dihydropyrimidine-5-carbonitrile (**11d**).* White solid; (0.09 g, 77%). M. p. 228–230 °C. ^{1}H NMR (400 MHz, DMSO-d_6) δ 8.60 (s, 1H), 8.08 (s, 1H), 7.65 (d, J = 8.7 Hz, 2H), 7.00 (d, J = 8.7 Hz, 2H), 3.82 (s, 3H), 2.66 (s, 3H). ^{13}C NMR (101 MHz, DMSO-d_6) δ 170.6, 167.4, 167.2, 164.5, 161.3, 155.3, 154.9, 143.6, 130.1, 129.5, 120.0, 115.1, 114.0, 90.8, 55.8, 25.2. GC-MS EI m/z (%): 391.02 (M^+, 16.18). Anal. calcd for $C_{18}H_{13}N_7O_2S$ (391.09): C, 55.23; H, 3.35; N, 25.05. Found: C, 55.11; H, 3.30; N, 25.09%.

*4.1.4.5 4-(3,4-Dimethoxyphenyl)-2-((5-methyl-[1,2,4]triazolo [1,5-a]pyrimidin-7-yl)thio)-6-oxo-1,6-dihydropyrimidine-5-carbonitrile (**11e**).* White solid; (0.089 g, 71%). M. p. 236–238 °C. ^{1}H NMR (400 MHz, DMSO-d_6) δ 8.84 (s, 1H), 8.54 (s, 1H), 7.81 (s, 1H), 6.91 (d, J = 8.3 Hz, 1H), 6.87 (d, J = 1.7 Hz, 1H), 6.78 (dd, J = 8.2, 1.7 Hz, 1H), 5.41 (s, 1H), 4.79 (d, J = 3.4 Hz, 1H), 3.74 (d, J = 1.2 Hz, 6H), 2.15 (s, 3H). ^{13}C NMR (101 MHz, DMSO-d_6) δ 189.5, 176.2, 174.0, 167.3, 161.7, 160.7, 157.1, 151.9, 148.9, 148.3, 139.0, 126.8, 118.6, 112.0, 110.9, 95.0, 57.0, 56.1, 24.6. GC-MS EI m/z (%): 420.92 (M^+, 15.78). Anal. calcd for $C_{19}H_{15}N_7O_3S$ (421.10): C, 54.15; H, 3.59; N, 23.27. Found: C, 54.12; H, 3.48; N, 23.21%.

*4.1.4.6 4-(3-Bromophenyl)-2-((5-methyl-[1,2,4]triazolo[1,5-a] pyrimidin-7-yl)thio)-6-oxo-1,6-dihydropyrimidine-5-carbonitrile (**11f**).* White solid; (0.088 g, 67%). M. p. 250–252 °C. ^{1}H NMR (400 MHz, DMSO-d_6) δ 8.56 (s, 1H), 7.95 (s, 1H), 7.90 (s, 1H), 7.65 (d, J = 8.1 Hz, 1H), 7.55 (s, 1H), 7.39 (t, J = 7.9 Hz, 1H), 2.65 (s, 3H). ^{13}C NMR (101 MHz, DMSO-d_6) δ 173.1, 170.1, 167.6, 166.1, 164.5, 161.7, 158.6, 151.9, 139.5, 133.3, 131.1, 127.5, 121.9, 119.3, 115.4, 95.1, 24.6. GC-MS EI m/z (%): 438.85 (M^+, 20.36). Anal. calcd for $C_{17}H_{10}BrN_7OS$ (438.99): C, 46.38; H, 2.29; N, 22.27. Found: C, 46.36; H, 2.20; N, 22.18%.

4.1.5 General procedure for the preparation of oxadiazole derivatives (13a–e). Appropriate thiol derivatives **12a–e** (0.05 mmole) with K_2CO_3 (1.5 eq.) in dioxane were stirred at rt for 30 min. Then, the corresponding chloride (0.05 mmole) was added. The resulting mixture was refluxed overnight. The reaction mixture was poured into crushed ice, the solid precipitated was filtered and washed with water.

*4.1.5.1 2-((5-Methyl-[1,2,4]triazolo[1,5-a]pyrimidin-7-yl)thio)-5-phenyl-1,3,4-oxadiazole (**13a**).* White solid; (0.08 g, 86%). M. p. 260–262 °C. ^{1}H NMR (400 MHz, DMSO-d_6) δ 8.70 (s, 1H), 8.12–8.04 (m, 2H), 7.76–7.65 (m, 3H), 7.39 (s, 1H), 2.59 (s, 3H). ^{13}C NMR (101 MHz, DMSO-d_6) δ 168.3, 165.5, 156.0, 155.5, 154.7, 142.8, 133.2, 130.0, 127.5, 123.4, 110.6, 25.2. GC-MS EI m/z (%): 310.21 (M^+, 23.60). Anal. calcd for $C_{14}H_{10}N_6OS$ (310.06): C, 54.18; H, 3.25; N, 27.08. Found: C, 54.25; H, 3.20; N, 27.11%.

*4.1.5.2 2-((5-Methyl-[1,2,4]triazolo[1,5-a]pyrimidin-7-yl)thio)-5-(p-tolyl)-1,3,4-oxadiazole (**13b**).* White solid; (0.071 g, 73%). M. p. 240–242 °C. ^{1}H NMR (400 MHz, DMSO-d_6) δ 8.70 (s, 1H), 7.97 (d, J = 8.0 Hz, 2H), 7.46 (d, J = 8.0 Hz, 2H), 7.37 (s, 1H), 2.58 (s, 3H), 2.43 (s, 3H). ^{13}C NMR (101 MHz, DMSO-d_6) δ 168.4, 165.5, 156.0, 155.2, 154.7, 143.6, 142.9, 130.6, 127.4, 120.7, 110.5, 25.2, 21.7. GC-MS EI m/z (%): 323.95 (M^+, 24.31). Anal. calcd for $C_{15}H_{12}N_6OS$ (324.08): C, 55.54; H, 3.73; N, 25.91. Found: C, 55.36; H, 3.70; N, 25.88%.

*4.1.5.3 2-((5-Methyl-[1,2,4]triazolo[1,5-a]pyrimidin-7-yl)thio)-5-(4-nitrophenyl)-1,3,4-oxadiazole (**13c**).* White solid; (0.074 g, 70%). M. p. 264–266 °C. ^{1}H NMR (400 MHz, DMSO-d_6) δ 8.70 (s, 1H), 8.48 (d, J = 8.9 Hz, 2H), 8.35 (d, J = 8.9 Hz, 2H), 7.45 (s, 1H), 2.59 (s, 3H). ^{13}C NMR (101 MHz, DMSO-d_6) δ 166.9, 165.5, 156.9, 156.0, 154.7, 150.1, 142.3, 128.9, 128.9, 125.2, 110.9, 25.2. GC-MS EI m/z (%): 355.31 (M^+, 19.15). Anal. calcd for $C_{14}H_9N_7O_3S$ (355.05): C, 47.32; H, 2.55; N, 27.59. Found: C, 47.18; H, 2.39; N, 27.52%.

*4.1.5.4 2-(4-Chlorophenyl)-5-((5-methyl-[1,2,4]triazolo[1,5-a] pyrimidin-7-yl)thio)-1,3,4-oxadiazole (**13d**).* White solid; (0.067 g, 65%). M. p. 258–260 °C. ^{1}H NMR (400 MHz, DMSO-d_6) δ 8.70 (s, 1H), 8.10 (d, J = 8.6 Hz, 2H), 7.74 (d, J = 8.6 Hz, 2H), 7.40 (s, 1H), 2.58 (s, 3H). ^{13}C NMR (101 MHz, DMSO-d_6) δ 167.6, 165.5, 156.0, 155.8, 154.7, 142.7, 138.0, 130.2, 129.3, 122.3, 110.6, 25.2. GC-MS EI m/z (%): 343.92 (M^+, 21.22). Anal. calcd for $C_{14}H_9ClN_6OS$ (344.02): C, 48.77; H, 2.63; N, 24.38. Found: C, 48.70; H, 2.52; N, 24.39%.

*4.1.5.5 2-(4-Bromophenyl)-5-((5-methyl-[1,2,4]triazolo[1,5-a] pyrimidin-7-yl)thio)-1,3,4-oxadiazole (**13e**).* White solid; (0.078 g, 67%). M. p. 270–272 °C. ^{1}H NMR (400 MHz, DMSO-d_6) δ 8.69 (s, 1H), 8.01 (d, J = 8.4 Hz, 2H), 7.88 (d, J = 8.4 Hz, 2H), 7.40 (s, 1H),

2.59 (s, 3H). ^{13}C NMR (101 MHz, DMSO-d_6) δ 167.6, 165.3, 156.0, 155.6, 154.2, 142.7, 134.5, 131.0, 128.0, 122.3, 110.6, 25.2. GC-MS EI m/z (%): 387.92 (M^+, 19.02). Anal. calcd for $C_{14}H_9BrN_6OS$ (387.97): C, 43.20; H, 2.33; N, 21.59. Found: C, 43.15; H, 2.3.; N, 21.69%.

4.2. Biological evaluation

4.2.1. Antiproliferative screening. Using the MTT assay, which has been used in the literature, the new TP hybrids' *in vitro* anticancer activity was assessed.[42,43]

4.2.2. *In vitro* multiple kinase inhibitory assay. The enzyme assays were done as described in the literature.[42,44]

4.2.3. Flow cytometry analysis of the cell cycle distribution. According to reports, it was done using MCF-7 cell lines that had been labeled with PI and examined using a FACS calibur flow cytometer.[42,43,45]

4.2.4. Cell apoptosis analysis. Using MCF-7 cells and the Annexin V-FITC/PI apoptosis detection kit, the degree of apoptosis was assessed in accordance with the published protocol.[42,46,47]

4.2.5. *In vivo* anti-breast cancer activity assay of 13c compound and its effect on the apoptotic marker (caspase-3) level. The Mansoura University Faculty of Pharmacy's research and ethics committee approved the *in vivo* anti-breast cancer assay technique for use in clinical investigations. Also, it was approved by Mansoura University Animal Care and Use Committee Code number: MU-ACUC (PHARM.MS.23.02.8). The *in vivo* anti-breast cancer activity of compounds **13c** was evaluated using the reported method in the literature.[37] After that, the samples were stained with hematoxylin and eosin (H&E) and caspase-3 immunostain, and then histopathological and immunohistochemical studies were performed. ImageJ software was used to quantify the caspase-3 immunostaining, and the data were presented as mean ± standard error ($n = 5$). Using SPSS 20 software (SPSS Inc., Chicago, IL), statistical analyses included one-way ANOVA and Tukey's *post hoc* test for multiple comparisons against the control group. Less than 0.05 was the threshold for statistical significance.[37]

4.3. Molecular docking study

To investigate the binding mode of the most active compounds in comparison to the co-crystallized ligand, molecular docking was utilized to obtain insights on their interaction with the active site of EGFR, HER-2, TOP-II and aromatase enzyme. Hence, their crystal structures were obtained from PDB using the codes: 4WKQ, 3PP0, 1ZXM and 3S79 respectively. Using Protein Repair and Analysis Server, the obtained 3D structures were produced by assigning bond ordering, adding missing atoms, optimizing hydrogen bonds, and correcting charges.[48] After that, the co-crystallized ligand and water molecules were eliminated. For virtual screening, the protein's produced PDB file was loaded into PyRx software's protein preparation module,[49–51] where they were converted to pdbqt files and the active sites were defined as grid box size was 20 × 20 × 20 and the coordinates were for EGFR was X: 2.715 Y: 194.363 Z: 20.975 while for HER-2 was X: 2.715 Y: 194.363 Z: 20.975, in case of TOP-II, X: 65.444 Y: 18.789 Z: 28.34, finally, the coordinates for aromatase were: X: 84.35 Y: 50.9 Z: 43.68.

Compounds **13c**, **11e** and **7c** were obtained as mol files using Marvin sketch version 21.17.0, ChemAxon (**https://www.chemaxon.com**) which were converted to Pdbqt format using ligand preparation module integrated in PyRx. Autodock vina was used as the engine for the molecular docking study, using default parameters where exhaustiveness was 12 and 3 poses were selected for post-docking analysis based on their binding free energy (ΔG), and the docked poses were subjected to analysis to determine how they bind with the active site using Discovery studio visualizer, where 2D and 3D presentation of ligand protein complexes were generated.[52,53]

Data availability

Upon reasonable request, the data supporting the conclusions of this study can be obtained from the corresponding author, S. S. T.

Conflicts of interest

The authors declare no conflicts of interest.

Acknowledgements

The authors reported there is no funding associated with the work featured in this article.

References

1 S. Zhang, H. Xu, L. Zhang and Y. Qiao, *Chin. J. Cancer Res.*, 2020, **32**, 720.
2 N. L. Dashputre, J. D. Kadam, U. D. Laddha, S. B. Patil, P. B. Udavant and S. P. Kakad, *Eur. J. Med. Chem. Rep.*, 2023, **9**, 100116.
3 S. Łukasiewicz, M. Czeczelewski, A. Forma, J. Baj, R. Sitarz and A. Stanisławek, *Cancers*, 2021, **13**, 4287.
4 C. K. Chan, G. Aimagambetova, T. Ukybassova, K. Kongrtay and A. Azizan, *J. Oncol.*, 2019, **2019**, 3257939.
5 A. Hamdi, E. Said, A. A Farahat, S. AA El-Bialy and M. AM Massoud, *Lett. Drug Des. Discovery*, 2016, **13**, 912–920.
6 M. Oshi, S. Gandhi, Y. Tokumaru, L. Yan, A. Yamada, R. Matsuyama, T. Ishikawa, I. Endo and K. Takabe, *Am. J. Cancer Res.*, 2021, **11**, 5094.
7 M. T. Pagano, E. Ortona and M. L. Dupuis, *Front. Endocrinol.*, 2020, **11**, 506.
8 X. Li, L. Zhao, C. Chen, J. Nie and B. Jiao, *Biochim. Biophys. Acta*, 2022, **1877**, 188789.
9 E. Rubin, K. S. Shan, S. Dalal, D. U. D. Vu, A. M. Mililllo-Naraine, D. Guaqueta and A. Ergle, *Int. J. Mol. Sci.*, 2024, **25**, 1064.
10 A. Magnifico, L. Albano, S. Campaner, D. Delia, F. Castiglioni, P. Gasparini, G. Sozzi, E. Fontanella, S. Menard and E. Tagliabue, *Clin. Cancer Res.*, 2009, **15**, 2010–2021.
11 P. H. Lin and G. Laliotis, *J. Clin. Med.*, 2022, **11**, 5891.

12 D. Molehin, F. Rasha, R. L. Rahman and K. Pruitt, *Mol. Cell. Biochem.*, 2021, **476**, 2449–2464.
13 P. Ratre, K. Mishra, A. Dubey, A. Vyas, A. Jain and S. Thareja, *Anti-Cancer Agents Med. Chem.*, 2020, **20**, 1994–2004.
14 C. P. Amaro, A. Batra and S. Lupichuk, *Curr. Oncol.*, 2021, **28**, 2270–2280.
15 A. M. Farghaly, O. M. AboulWafa, H. H. Baghdadi, H. A. Abd El Razik, S. M. Y. Sedra and M. M. Shamaa, *Bioorg. Chem.*, 2021, **115**, 105208.
16 M. Ogino, T. Fujii, Y. Nakazawa, T. Higuchi, Y. Koibuchi, T. Oyama, J. Horiguchi and K. Shirabe, *In Vivo*, 2020, **34**, 3483–3487.
17 Y. Wu, Y. Han, Q. Li, P. Zhang, P. Yuan, Y. Luo, Y. Fan, S. Chen, R. Cai and Q. Li, *Breast Cancer Res. Treat.*, 2022, **193**, 381–392.
18 J. Y. Jang, D. Kim and N. D. Kim, *Int. J. Mol. Sci.*, 2023, **24**, 8457.
19 K. Oukoloff, B. Lucero, K. R. Francisco, K. R. Brunden and C. Ballatore, *Eur. J. Med. Chem.*, 2019, **165**, 332–346.
20 C. M. Richardson, D. S. Williamson, M. J. Parratt, J. Borgognoni, A. D. Cansfield, P. Dokurno, G. L. Francis, R. Howes, J. D. Moore and J. B. Murray, *Bioorg. Med. Chem. Lett.*, 2006, **16**, 1353–1357.
21 H. S. Mohamed, N. H. Amin, M. T. El-Saadi and H. M. Abdel-Rahman, *Bioorg. Chem.*, 2022, **121**, 105687.
22 X.-S. Huo, X.-E. Jian, J. Ou-Yang, L. Chen, F. Yang, D.-X. Lv, W.-W. You, J.-J. Rao and P.-L. Zhao, *Eur. J. Med. Chem.*, 2021, **220**, 113449.
23 C. J. A. Ribeiro, J. Kankanala, J. Xie, J. Williams, H. Aihara and Z. Wang, *Bioorg. Med. Chem. Lett.*, 2019, **29**, 257–261.
24 S. Wang, L.-J. Zhao, Y.-C. Zheng, D.-D. Shen, E.-F. Miao, X.-P. Qiao, L.-J. Zhao, Y. Liu, R. Huang and B. Yu, *Eur. J. Med. Chem.*, 2017, **125**, 940–951.
25 S. Wang, Z.-R. Li, F.-Z. Suo, X.-H. Yuan, B. Yu and H.-M. Liu, *Eur. J. Med. Chem.*, 2019, **167**, 388–401.
26 D. H. Dawood, E. S. Nossier, M. M. Ali and A. E. Mahmoud, *Bioorg. Chem.*, 2020, **101**, 103916.
27 S. T. J. Bradford, E. Grimley, A. M. Laszczyk, P. H. Lee, S. R. Patel and G. R. Dressler, *Cell Chem. Biol.*, 2022, **29**, 412–422.
28 T. Heinrich, H.-P. Buchstaller, B. Cezanne, F. Rohdich, J. Bomke, M. Friese-Hamim, M. Krier, T. Knöchel, D. Musil, B. Leuthner and F. Zenke, *Bioorg. Med. Chem. Lett.*, 2017, **27**, 551–556.
29 X.-J. Dai, L.-P. Xue, S.-K. Ji, Y. Zhou, Y. Gao, Y.-C. Zheng, H.-M. Liu and H.-M. Liu, *Eur. J. Med. Chem.*, 2023, **249**, 115101.
30 S. M. Gomha, F. M. Abdelrazek and M. M. Abdulla, *J. Chem. Res.*, 2015, **39**, 425–429.
31 M. J. Akhtar, A. A. Siddiqui, A. A. Khan, Z. Ali, R. P. Dewangan, S. Pasha and M. S. Yar, *Eur. J. Med. Chem.*, 2017, **126**, 853–869.
32 H. T. Abdel-Mohsen, F. A. Ragab, M. M. Ramla and H. I. El Diwani, *Eur. J. Med. Chem.*, 2010, **45**, 2336–2344.
33 A. Faraji, R. Motahari, Z. Hasanvand, T. O. Bakhshaiesh, M. Toolabi, S. Moghimi, L. Firoozpour, M. A. Boshagh, R. Rahmani and S. H. Ketabforoosh, *Bioorg. Chem.*, 2021, **108**, 104553.
34 M. N. Aboul-Enein, A. M. A. E. S. El-Azzouny, F. A. F. Ragab and M. F. Hamissa, *Arch. Pharm.*, 2017, **350**, 1600377.
35 E. Jameel, P. Meena, M. Maqbool, J. Kumar, W. Ahmed, S. Mumtazuddin, M. Tiwari, N. Hoda and B. Jayaram, *Eur. J. Med. Chem.*, 2017, **136**, 36–51.
36 W. A. Ewes, S. S. Tawfik, A. M. Almatary, M. Ahmad Bhat, H. W. El-Shafey, A. A. Mohamed, A. Haikal, M. A. El-Magd, A. A. Elgazar and M. Balaha, *Molecules*, 2024, **29**, 3186.
37 M. A. Sabry, M. A. Ghaly, A. R. Maarouf and H. I. El-Subbagh, *Eur. J. Med. Chem.*, 2022, **241**, 114661.
38 D. I. A. Othman, A. Hamdi, S. S. Tawfik, A. A. Elgazar and A. S. Mostafa, *J. Enzyme Inhib. Med. Chem.*, 2023, **38**, 2166037.
39 M. T. E. Maghraby, T. Mazyad Almutairi, S. Bräse, O. I. A. Salem, B. G. M. Youssif and M. M. Sheha, *Molecules*, 2023, **28**, 7092.
40 K. Pandey, K. Bharat Lokhande, A. Saha, A. Goja, K. V. Swamy and S. Nagar, *Curr. Comput.-Aided Drug Des.*, 2023, **19**, 243–257.
41 M. M. Al-Sanea, A. Hamdi, A. A. Mohamed, H. W. El-Shafey, M. Moustafa, A. A. Elgazar, W. M. Eldehna, H. Ur Rahman, D. G. Parambi and R. M. Elbargisy, *J. Enzyme Inhib. Med. Chem.*, 2023, **38**, 2166036.
42 N. F. El Hamaky, A. Hamdi, W. A. Bayoumi, A. A. Elgazar and M. N. Nasr, *Bioorg. Chem.*, 2024, **148**, 107437.
43 T. Mosmann, *J. Immunol. Methods*, 1983, **65**, 55–63.
44 S. S. Tawfik, A. Hamdi, A. R. Ali, A. A. Elgazar, H. W. El-Shafey, A. S. El-Azab, A. H. Bakheit, M. M. Hefnawy, H. A. Ghabbour and A.-M. Alaa, *RSC Adv.*, 2024, **14**, 26325–26339.
45 F. Tavakolinia, T. Baghipour, Z. Hossaini, D. Zareyee, M. A. Khalilzadeh and M. Rajabi, *Nucleic Acid Ther.*, 2012, **22**, 265–270.
46 M. Kusaczuk, R. Krętowski, M. Naumowicz, A. Stypułkowska and M. Cechowska-Pasko, *Int. J. Nanomed.*, 2018, 2279–2294.
47 D. I. Othman, A. Hamdi, W. M. Elhusseiny, A. S. El-Azab, A. H. Bakheit, M. Hefnawy and A.-M. Alaa, *Saudi Pharm. J.*, 2023, **31**, 101803.
48 O. S. Nnyigide, T. O. Nnyigide, S.-G. Lee and K. J. J. o. C. I. Hyun, *Modeling*, 2022, **62**, 4232–4246.
49 A. A. Elgazar, R. A. El-Domany, W. M. Eldehna and F. A. Badria, *ACS Omega*, 2023, **8**, 39490–39510.
50 A. Hamdi, M. Yaseen, W. A. Ewes, M. A. Bhat, N. I. Ziedan, H. W. El-Shafey, A. A. B. Mohamed, M. R. Elnagar, A. Haikal, D. I. A. Othman, A. A. Elgazar, A. H. A. Abusabaa, K. S. Abdelrahman, O. M. Soltan and M. M. Elbadawi, *J. Enzyme Inhib. Med. Chem.*, 2023, **38**, 2231170.
51 A. A. Elgazar, R. A. El-Domany, W. M. Eldehna and F. A. Badria, *RSC Adv.*, 2023, **13**, 25616–25634.
52 F. F. El-Senduny, A. A. Elgazar, H. A. Alwasify, A. Abed, M. Foda, S. Abouzeid, L. Lewerenz, D. Selmar and F. Badria, *Planta Med.*, 2023, **89**, 964–978.
53 M. M. Al-Sanea, G. Chilingaryan, N. Abelyan, M. Mamikonyan, H. Gasparyan, S. Hovhannisyan, A. Hamdi, A. R. Ali, S. Selim and A. A. Mohamed, *PLoS One*, 2022, **17**, e0272065.